QUEEN'S UNIVERSITY BELFAST

Sampling methods based on expected traffic-volume information for long-term rotation-based bridge SHM in resource-constrained environments

Ferguson, A. J., O'Higgins, C., Hester, D., & Woods, R. (2024). Sampling methods based on expected traffic-volume information for long-term rotation-based bridge SHM in resource-constrained environments. *Mechanical Systems and Signal Processing*, *208*, Article 110933. https://doi.org/10.1016/j.ymssp.2023.110933

Published in:
Mechanical Systems and Signal Processing

Document Version:
Publisher's PDF, also known as Version of record

Queen's University Belfast - Research Portal:
Link to publication record in Queen's University Belfast Research Portal

Publisher rights
Copyright 2023 The Authors.

This is an open access article published under a Creative Commons Attribution License (https://creativecommons.org/licenses/by/4.0/), which permits unrestricted use, distribution and reproduction in any medium, provided the author and source are cited.

General rights
Copyright for the publications made accessible via the Queen's University Belfast Research Portal is retained by the author(s) and / or other copyright owners and it is a condition of accessing these publications that users recognise and abide by the legal requirements associated with these rights.

Take down policy
The Research Portal is Queen's institutional repository that provides access to Queen's research output. Every effort has been made to ensure that content in the Research Portal does not infringe any person's rights, or applicable UK laws. If you discover content in the Research Portal that you believe breaches copyright or violates any law, please contact openaccess@qub.ac.uk.

Open Access
This research has been made openly available by Queen's academics and its Open Research team. We would love to hear how access to this research benefits you. – Share your feedback with us: http://go.qub.ac.uk/oa-feedback

Download date:04. Jun. 2024

Mechanical Systems and Signal Processing 208 (2024) 110933

Contents lists available at ScienceDirect

Mechanical Systems and Signal Processing

journal homepage: www.elsevier.com/locate/ymssp

Sampling methods based on expected traffic-volume information for long-term rotation-based bridge SHM in resource-constrained environments

Alan J. Ferguson [a,b,*], Connor O'Higgins [a], David Hester [a], Roger Woods [b]

[a] School of Natural and Built Environment, Queen's University Belfast, David Keir Building, Stranmillis Road, Belfast, BT9 5AG, UK
[b] School of Electronics, Electrical Engineering, and Computer Science, Queen's University Belfast, Ashby Building, Stranmillis Road, Belfast, BT9 5AG, UK

ARTICLE INFO

Communicated by W.-X. Ren

Keywords:
Bridge structural health monitoring
Rotation-based damage detection
Long-term monitoring
Sampling methods
Expected traffic volume based sampling

ABSTRACT

Effective bridge structural health monitoring systems offer a route to assist in the safe and economic operation of bridges, but have seen limited adoption onto the short and medium-span bridges which represent the majority of our bridge stock. This lack of adoption is in part due to the practical challenges of deploying bridge SHM systems in resource-constrained environments, especially where long-term monitoring at transport network-scales is considered. This paper tackles the problem of implementing an effective sampling method to facilitate long-term, bridge rotation-based damage detection, particularly within the confines of a resource-constrained setting. We demonstrate that leveraging readily available expected traffic-volume information enables the creation of more effective bridge SHM sampling methods by capturing more vehicle crossings in the same time. Furthermore, we introduce an empirically tuned, temperature-capable bridge finite-element model for long-term simulations, incorporating a stochastic vehicle arrival model and a feature error model to allow for the presence of any residual noise/dynamics due to imperfect filtering or inaccuracies in the feature extraction stages. This allowed us to simulate 60 years worth of bridge rotation monitoring data with varying damage severities to evaluate the impact of environmental and operational variations on our proposed expected traffic volume based sampling methods. Our results show that sampling only the peak traffic hours was the most effective for the same reduced 'on' time, i.e. for an 8x reduction in 'on' time only a 1.5x increase in the minimum detectable damage was observed versus a 2x increase for naive random sampling.

1. Introduction

Bridge design working lifespans are typically 100 years or more [1], thus making long-term bridge inspection and management processes crucial. Conventionally, these rely on periodic visual inspections by engineers [2]. Bridge structural health monitoring (BSHM) uses quantitative sensor data and automation to offer the possibility of both enhanced diagnostic and prognostic capabilities. Adopting BSHM technologies provides a potentially promising avenue to augment existing "visual inspection only" regimes, however, it bears noting that its deployment is currently typically limited to long-span structures.

* Corresponding author at: School of Natural and Built Environment, Queen's University Belfast, David Keir Building, Stranmillis Road, Belfast, BT9 5AG, UK.
E-mail addresses: a.j.ferguson@qub.ac.uk (A.J. Ferguson), c.ohiggins@qub.ac.uk (C. O'Higgins), d.hester@qub.ac.uk (D. Hester), r.woods@qub.ac.uk (R. Woods).

https://doi.org/10.1016/j.ymssp.2023.110933
Received 1 June 2023; Received in revised form 10 September 2023; Accepted 6 November 2023
Available online 22 November 2023
0888-3270/© 2023 The Author(s). Published by Elsevier Ltd. This is an open access article under the CC BY license (http://creativecommons.org/licenses/by/4.0/).

Deploying these BSHM systems comes with various challenges mainly due to resource constraints, particularly when viewed at the scale of entire transport networks, considering the multitude of short and medium span structures that make up the majority of our bridge stock. In this context, we consider these "resource-constrained environments" to encompass not only technological barriers, such as potentially restricted or intermittent energy sources and data transmission capabilities, but also economic and environmental considerations, where crucially these constraints are interlinked. For example, lowering energy requirements could lead to designs using smaller energy sources, such as self-powered energy harvesting devices; in turn, this could reduce financial costs and help minimise the embodied and operational carbon footprint of these systems. Furthermore, given the ever increasing financial budgetary pressures faced by bridge owners and operators, even such small efficiencies can significantly impact the feasibility of deploying BSHM systems at transport network-scales.

Our key observation is that sampling techniques typically developed for wireless sensor network (WSN) applications [3] align well with the challenges of BSHM, due to their focus on reducing the energy consumption used when measuring time-series sensor data. These methods allow the embedded system hardware to enter lower-power states (commonly referred to as sleep or idle) during inactive periods, thus reducing energy consumption. It should be noted that BSHM typically requires continual recording during vehicle crossings unlike many WSN applications such as [4], where sensor systems can wake up and take a single measurement and go back to sleep. As a consequence, sampling methods for BSHM systems are likely to require the system to remain in the higher-power, active ('on') state for longer. Furthermore, a trade-off for sampling-based BSHM approaches would be that their reduced feature data volumes could result in reduced damage detection capability.

In spite of these challenges, in this paper, we demonstrate that incorporating basic information about expected traffic volumes into our sampling methods can offer improved damage detection performance versus naive random sampling approaches. Traffic-volume information allows these sampling algorithms to capture more vehicle crossings for the same 'on' time, by focusing on time-periods with higher expected traffic volumes. In particular, the information used, i.e. the expected average traffic counts for each hour, would require no additional instrumentation and can be obtained easily in advance of deployment, both of which improve its suitability for implementing on low-cost embedded sensor systems.

In this paper, we consider the specific example of a rotation-based damage detection system on a typical highway bridge and investigate the application of both our traffic-volume information based sampling methods and a naive random sampling approach. Rotation-based bridge SHM approaches have became more widely used due to the more recent availability of relatively low cost direct current (DC) micro-electromechanical systems (MEMS) accelerometers capable of monitoring the relatively small rotation transients on short-span bridges under vehicle loading.

Rigorously evaluating the likely damage detection capabilities of these sampling methods requires long-term bridge rotation data with known damage states, as well as realistic levels of environmental and operation variation. As carrying out long-term in situ testing on live bridge structures with damage evolution is broadly infeasible, there exists only very limited data for these types of full-scale studies. Hence, most rotation-based BSHM work to date has been validated using numerical models or laboratory-scale experiments, which often do not account for long-term confounding effects, such as diurnal and seasonal temperature variation. Therefore, in this work, a method for simulating the required long-term bridge rotation data is proposed by developing an empirically tuned, temperature capable bridge finite-element (FE) model, which captures a realistic level of variation in structural stiffness state caused by diurnal and seasonal temperature variation.

Specifically, our long-term bridge simulation approach is based on: (a) developing an updated FE model of the bridge so that the mode shapes and frequencies predicted by the FE model match the values measured experimentally during a modal test; (b) long-term air temperature and bridge natural frequency measurements collected on the bridge allowed the creation of a time-series data model that can reliably predict a bridge natural frequency from air temperature measurements; and (c) a transformation that is fitted between bridge natural frequency values and corresponding Young's modulus (E) values via an FE model tuning procedure. Thus, the transformed time-series data model's output for a given air temperature time-series is a corresponding E value time-series that can be applied to an FE model for long-term numerical simulations to incorporate a more realistic level of seasonal and diurnal stiffness variation. Furthermore, a stochastic model for vehicle arrivals in free-flow traffic based on a dataset consisting of one year's worth of weigh-in-motion (WIM) records is used to generate realistic temporal distributions of vehicles (axle weights and spacings). Finally, an error model is applied to the rotation features used for damage detection (peak amplitude). This error model is used to account for the presence of residual noise or bridge–vehicle dynamics due to imperfect filtering, as well as any inaccuracy introduced by the peak prominence extraction algorithm.

The main contributions of this work are:

- Development of an empirically tuned, temperature capable FE model which allows the confounding effect of temperature variation to be investigated on any proposed bridge damage detection method, thereby permitting realistic long-term simulations that are not common in BSHM;
- Creation of a stochastic model for vehicle loading based on a WIM dataset that captures a realistic temporal distribution of vehicles with varying axle numbers and weights.
- Development of several potentially useful adaptive sampling algorithms based on expected traffic-volume information with their performance subsequently evaluated using numerical simulations of 60 years worth of healthy and damaged bridge data.

The remainder of this paper is organised as follows: Section 2 provides an overview of relevant previous work in the area of rotation-based bridge damage detection. Section 3 describes the bridge rotation-based damage detection approach using the Earth Movers' Distance which has been adopted in this study. Section 4 presents the numerical models used to simulate long-term bridge data with confounding effects due to environmental and loading variation. Section 5 sets out a number of candidate algorithms

for sampling to permit operation in a resource-constrained environment. Subsequently, Section 6 employs the new environmentally capable FE model to generate response data to test the performance of the sampling algorithms in long-term damage scenarios. Finally, Section 7 presents a discussion of these results, and Section 8 sets out the conclusions of this work.

2. Background

To set the context for this work, we cover the main approaches for bridge damage detection using rotation measurements. These can be categorised as follows: (1) rotation influence line (IL) approaches, and (2) rotation-based bridge WIM approaches, with each of these described presently. This allows the performance of our sampling methods to be compared against the typical levels of damage detectable in our rotation-based bridge SHM work for short to medium span bridges.

Rotation ILs can be measured directly using a vehicle of known weight [5] and in some studies, have been used to infer both the existence and location of damage in a structure. Zeinali et al. [6,7] proposed an approach for damage detection of beams using flexural rigidity estimation based on rotation ILs, where the rotation was measured at the supports using chequer board targets which were tracked using computer vision. Whilst the authors showed damage detection and localisation in spite of noise, the laboratory scale demonstration uses a simply supported slender steel bar which showed levels of rotation around $3.5\,\mathrm{mrad\,kN^{-1}}$, which is more than an order of magnitude greater than the level of rotation one would expect on a simply supported bridge span. Hence, based on the measurement approach and the magnitude of rotation simulated, it is very hard to infer how this approach would perform on a realistic full-scale bridge structure.

Hester et al. [8] proposed the difference between rotation ILs obtained for both healthy and damaged states to detect and localise damage, using the bridge response for a vehicle of known weight. This work showed that for a simply supported bridge that the most effective sensor locations are over the supports, as this corresponds to the locations with the maximum rotation amplitudes. Laboratory-scale experiments [9] on a $5.4\,\mathrm{m}$ simply supported beam structure showed the difference of rotation ILs approach could detect damage as low as a 7% loss of stiffness over 2.5% of the span length. Alamdari et al. [10] proposed a similar damage detection approach based on the difference between rotation ILs in pre- and post-damage conditions, using simulations and laboratory tests.

Rotation-based bridge WIM, e.g. [11], has been proposed by some authors as a means for detecting damage. The approach presented by O'Brien et al. [12] was based on the overestimation of vehicle weights by a rotation-based bridge WIM system following damage. It showed that there is statistical repeatability in the tandem weights of five axle vehicles which can be used for bridge damage detection and that the level of sensitivity of rotation to damage is related to the distance of the measurement from the location of the damage. They proposed to address this issue by placing one inclinometer at each end of the bridge. Separately, Wei et al. [13] proposed the same approach as [12], but instead used two axle vehicles as the fluctuation form of their axle weight time history is more simple to analyse.

The limitations of the above work are: the additional instrumentation complexity incurred, e.g. requiring costly and relatively uncommon bridge WIM setups; the requirement for bridge closures to carry out static load tests for calibration; and the indirect approaches adopted by these approaches, necessitating calculating intermediate results such as ILs or axle weights.

This section has focused on studies which have used rotation measurements for bridge damage detection, of which there are not many, and a summary of these has been presented in Table 1.

3. Rotation-based bridge damage detection approach

Modern DC MEMS accelerometers have emerged as a cost-effective way to monitor the relatively small amplitude rotation transients typically observed under vehicle loading on short span bridges. Measuring rotation at the supports has been shown to be the most effective for detecting damage [12]. For the typical short span bridge considered in this work, this means that even a relatively sparse sensor network with DC MEMS accelerometers positioned at the ends of spans can be used for monitoring. The exact number of sensor nodes required can be varied depending on the operational needs and financial budget available to monitor the structure-under-test, but at a minimum, this would likely consist of two accelerometers (one at either end of span) placed under each traffic lane. If more sensor nodes can be deployed, it would be the next sparsest arrangement would consist of DC MEMS accelerometers be placed at both ends of each longitudinal bridge beam.

Assuming the axis of the sensor is oriented in the bridge's longitudinal direction, this acceleration signal can be filtered to extract the static rotation component. Under typical highway vehicle loading, for each crossing there will be a corresponding rotation transient. The approach used in this work uses the peak amplitude of these transients as the feature to be tracked to detect damage. The distributions of these rotation peak amplitudes are recorded over time, where a shift in distribution will be noted post-damage, for which the Earth Movers' Distance (EMD) is used to quantify the post-damage shift in the distributions of these rotation amplitudes [15]. Furthermore, as we subsequently describe for this particular scenario involving two one-dimensional distributions, there exists a closed form solution that is readily implementable on the sort of low-power microprocessor needed in a resource-constrained environment due to its relatively low computational cost. Thus, by using the EMD to quantifying this shift in the distribution, the presence of damage can be established.

The EMD, which in mathematics is also known as the first Mallows or Wasserstein distance, is given by:

$$\ell_1(u,v) = \inf_{\pi\in\Gamma(u,v)} \int_{\mathbb{R}\times\mathbb{R}} |x-y|\,d\pi(x,y), \tag{1}$$

Table 1
Summary of studies using bridge rotation for damage detection including equivalent damage level using the δ metric of Sinha et al. [14].

Study type	Bridge description	Damage used	Equivalent δ
Laboratory [6]	Simply-supported 532 mm long × 24.5 mm wide × 1.5 mm thick steel bar	55 mm long section with 38 % stiffness loss located at approximately third-span	0.15
Laboratory [7]	Propped cantilever with 680 mm long × 76.2 mm wide × 3.2 mm steel bar	40 % stiffness loss from 0.25 L to 0.35 L	0.16
1-D FE [8]	Simply supported 20 m long bridge and 10 m wide consisting of 9 No Y3 precast beams spaced at 1.25 m centres with a 160 mm thick deck slab	30% stiffness loss over 1 m (5% length) at quarter span	0.11
3-D FE [8]	20 m long by 10 m wide precast concrete and continuous slab bridge (support conditions unspecified)	3L/8 span location as 12.1% reduction in stiffness over 3 m length and 5 m width	0.11
Laboratory [9]	Simply supported 5.6 m long steel I-beam section oriented in the weak direction	Stiffening of 16%, 25%, and 50% over 7.5%, 5%, and 2.5% span lengths	0.06
3-D FE [10]	Cable-stayed 46.2 m long by 6.3 m wide bridge with 16 stay cables	Symmetric and asymmetric cable failures	N/A
1-D FE [12]	Simply supported 20 m long bridge and 10 m wide consisting of 9 No Y3 precast beams spaced at 1.25 m centres with a 160 mm thick deck slab	Localised stiffness loss over 1 m (5% length) at mid-span with severities: 10%, 30%, and 50%	0.03
3-D FE [12]	20 m long and 11 m wide simply supported bridge, composed of a 0.2 m thick solid slab and 0.9 m deep 10 beams spaced at 1 m apart	Damage modelled over 3 m length at L/4, L/2 and 3L/4 span locations (one at a time), in longitudinal direction 32% reduction in central 1 m and 10% in outer 1 m lengths, across half of the bridge width, i.e. full width of a traffic lane.	0.12
1-D FE [13]	20 m long bridge with elastic modulus of 206×10^6 kN m^{-2} and the section moment of inertia of 8.1×10^{-3} m^4.	5%–15% stiffness reduction over 1.5 m located at 3 m, 6 m, 10 m, and 14 m	0.12

where $\boldsymbol{\Gamma}(u, v)$ are the set of probability distributions on $\mathbb{R} \times \mathbb{R}$, with marginals, u and v. If U and V are the cumulative distribution functions of u and v, this also equals:

$$\ell_1(u, v) = \int_{-\infty}^{+\infty} |U - V|. \tag{2}$$

A fuller exposition of the above equations can be found in [16].

This work considers only one-dimensional, empirical distributions and these are a special case for which the EMD has an exact solution. If X and Y are empirical distributions of the two datasets, i.e. $X = \{x_1 \leq \cdots \leq x_n\}$ and $Y = \{y_1 \leq \cdots \leq y_n\}$, both of size n, then the EMD is calculated [17] as:

$$\mathrm{EMD}(X, Y) = \sum_{i=1}^{n} |x_i - y_i|. \tag{3}$$

It is evident that the application of Eq. (3) requires that both distributions are the same size. In practice, however, the distributions used in this application are relatively large, and thus, need to be resampled or binned to meet this requirement [17]. This, therefore, allows the EMD to be computed efficiently by even a relatively low-powered system, specifically, by: (1) obtaining the empirical distributions by sorting the rotation datasets; (2) resampling these distributions to have the same size, as both will be relatively large and will already approximately be the same size; this can be achieved simply and with minimal loss of accuracy by dropping samples from the larger distribution; and (3) calculating the EMD as the summation of the difference between these distributions. By using the EMD to quantify the shift between distributions, then the damage indicators, $\mathrm{DI}_{\mathrm{LL}}$, and $\mathrm{DI}_{\mathrm{RR}}$, are formulated as:

$$\mathrm{DI}_{\mathrm{LL}} = \mathrm{EMD}\left(L_0, L_i\right), \quad \text{and} \tag{4}$$

$$\mathrm{DI}_{\mathrm{RR}} = \mathrm{EMD}\left(R_0, R_i\right), \tag{5}$$

where L_i and R_i are the distribution of maximum rotation values at the left and right ends of the span for the ith year.

4. Long-term bridge simulation methods

To robustly test the sampling methods proposed here as a means of addressing the challenge of implementing a rotation-based BSHM approach in a resource-constrained environment, the appropriate numerical models to simulate long-term bridge rotation data with both environmental and loading variations were required. Specifically, Section 4.1 describes the bridge FE model and damage model used in this work, Section 4.2 presents the approach used to incorporate the effect of seasonal and diurnal environmental variation into this FE model, and Section 4.3 describes the method used to generate random vehicle arrivals over time to allow traffic loading to be applied to the FE model.

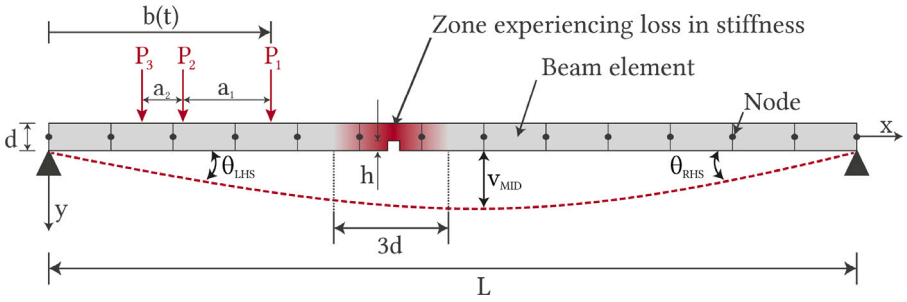

Fig. 1. Sketch of the beam discretised model subject to a 3-axle vehicle (point loads P_1, P_2, and P_3) with measurements for midspan displacement and LHS and RHS rotations indicated.

4.1. Bridge finite-element model

The numerical model used here is similar to that used in a number of other BSHM studies [18,19] (Fig. 1). The model has been created to approximate a typical 34 m span concrete beam and slab highway bridge. The simulated transverse width is slightly wider than one traffic lane to allow for some transverse load distribution into adjacent beams. This model was used as it represents a very common bridge type, and therefore is characteristic of many in-service bridges. Further work in [15] showed that the rotation response predicted by the model was consistent with the response measured on-site.

Despite a wide array of bridge damage mechanisms, one commonality is a resultant loss of structural stiffness, either globally, or locally. Hence, damage is introduced in the FE model by allowing for a localised loss in stiffness, e.g. due to a crack. A number of different crack damage models have been proposed, for instance, in the case of a vibrating cantilever, some studies have modelled a breathing crack [20]. However, when simulating damage to single span bridges under moving loads, this is commonly envisioned as a non-breathing crack. This is based on the assumption that the dead load of the bridges is large relative to the live load, which effectively maintains the crack in an open position.

The stiffness reduction used in this work is the one proposed by Sinha et al. [14] which quantifies a gradual loss of bending stiffness in the vicinity of the crack; specifically, for a beam with width, w, and depth, d, the loss of bending stiffness extends a distance, $l_c = 1.5d$, at both sides of the crack location, x_c. This loss of stiffness is modelled by introducing a reduced moment of inertia, I, in those elements close to a crack with height, h, as follows:

$$I(x) = \begin{cases} I_c + |x - x_c|\,(I_0 - I_c)/l_c, & \text{if } |x - x_c| \le l_c, \\ I_0, & \text{otherwise,} \end{cases} \tag{6}$$

where I_0 is the moment of inertia in the undamaged beam, and I_c denotes the reduced moment of inertia at the damage location, as described in [14].

Due to the fairly regular geometry of bridge beams and slabs, understandably much of the previous work on bridge elements envisage rectangular beams, where the ratio, $\delta = h/d$, has often been used to characterise the severity of the damage. Values of $\delta = 0.1$ and $\delta = 0.2$ represent localised losses in stiffness of 27.1 % and 48.8 % respectively of the inertia of a healthy rectangular section. The same equivalency between δ and associated percentage stiffness loss is maintained for the beam sections in this work and can be calculated as, $\%\ \text{Stiffness Loss} = \left(1 - (1-\delta)^3\right) \times 100$.

4.2. Environmentally capable bridge finite-element model under diurnal and seasonal variation

To capture the variation in structural stiffness due to both diurnal and seasonal temperature variation requires a FE model that can simulate this typical variation seen in structural stiffness. Whilst there is no direct, global measure of a structure's stiffness, tracking bridge natural frequencies is a recognised method of observing long-term trends in bridge stiffness [21]. These long-term trends in bridge stiffness can be observed as the measured bridge natural frequency is a function of the structure's geometry and material properties. For example, consider the equation for the first natural frequency, f_1, of an idealised simply supported beam:

$$f_1 = \frac{1}{2\pi}\sqrt{\frac{48EI}{ML^3}}, \tag{7}$$

where the mass, M, moment of inertia, I, and length, L, can all assumed to be invariant and any change in frequency will infer a change in Young's modulus, E.

If one had a way of reliably predicting the time-series of E values over several years, it would be possible to simulate this natural variation in stiffness in the FE model. The rotation or displacement values predicted by the FE model would then contain a realistic level of the confounding effect due to temperature. Herein, the approach proposed to predict the time-series of E values for a given temperature time-series, T, is as follows:

1. Development of an FE model that correctly predicts the mode shape and frequency measured during a modal test carried out at the start of the study;

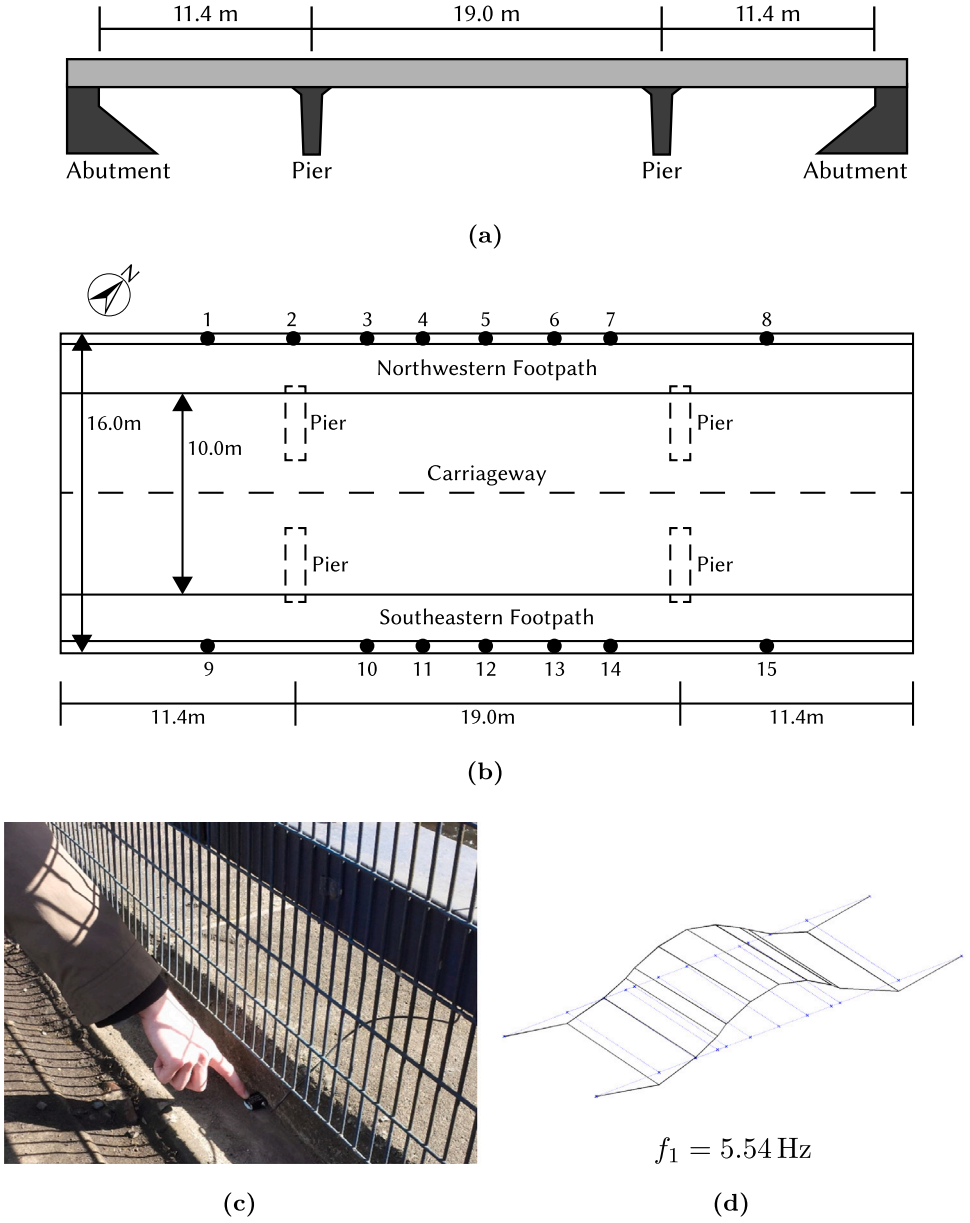

Fig. 2. (a) Sketches of the span dimensions of the bridge, (b) plan view of the bridge with schematic of the modal test instrumentation, (c) photograph of accelerometer location on pavement, and (d) plot showing the first mode shape and frequency obtained from the modal test.

2. Capture of a long-term dataset from the bridge consisting of: (a) bridge natural frequencies, which were extracted from ambient vibration data, and (b) hourly air temperature measurements covering the same period;
3. Fitting of a time-series data model to the long-term bridge frequency and temperature data, thereby allowing the first modal frequencies, $f_1[0] \dots f_1[n]$, to be predicted for a given sequence of hourly temperature data, $T[0] \dots T[n]$; and
4. Fitting a transformation between first modal frequencies and the corresponding $E[t]$ values using an FE model tuning process.

4.2.1. Bridge finite element model updating

As the focus of this study (and the vast majority of previous work) is on monitoring a single-span structure, ideally, there would be long-term frequency data available for such a bridge. However, due to the limited availability of long-term bridge frequency measurement data, we used the long term frequency data available to us, which, in this case, was for the three-span, two-lane wide, reinforced concrete slab bridge shown in Fig. 2. Thus, we will use this bridge data to develop a data model that can generate a

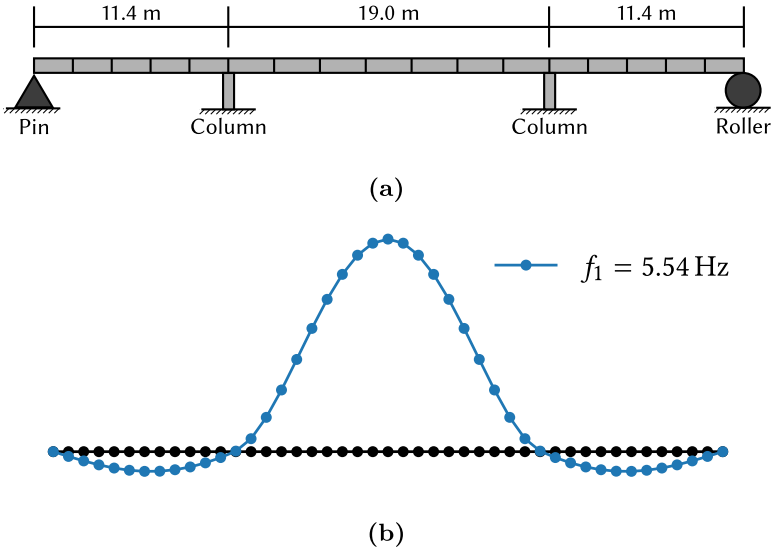

Fig. 3. Sketches of (a) the span dimensions of the bridge, (b) the idealised beam and supports used in the finite-element model; and (c) plot of the first mode shape predicted by the finite-element model.

realistic time series of Young's modulus (E) values for a concrete bridge based on air temperature time-series. Subsequently, this data model is used to generate E value time-series to be applied to the single-span reinforced concrete bridge model shown in Fig. 1.

The bridge consists of two 11.4 m long side spans, and an 19 m long centre span. The overall widths of the deck the carriageway are 16 m and 10 m respectively.

Bridge modal test

Prior to the long-term monitoring period, a modal test was carried out on the bridge. The test points were arranged as shown in Fig. 2(b). The accelerometers were mounted immediately adjacent to the parapet guard rail by temporarily gluing metal blocks onto the pavement as indicated in Fig. 2(c). The first mode shape is shown in Fig. 2(d), with the first modal frequency found to be 5.54 Hz.

Bridge finite element model

As shown in Fig. 3(a), the bridge has been idealised as a continuous beam with the two piers modelled as columns with fixed connections and pin-roller supports at the ends. The FE model used is the same as that described in [15]. In this FE model, several key assumptions have been made including that the material is homogeneous and exhibits linear elastic behaviour meaning that within the elastic limit, its stress and strain are directly proportional . Therefore, only small deformations can be modelled so as to stay below the elastic limit of the material. However, given that the load due to the passage of even a relatively heavy truck is within the ultimate limit state design loads for a bridge, such as specified by the Eurocode standards [22], then in all likelihood the bridge's response will be linear elastic for the type of loads we are modelling, i.e. free-flow traffic.

Furthermore, for simplicity, the geometry has been modelled as idealised, so any small defects or deviations have been ignored, and the boundary conditions are also modelled as idealised restraints. The pin supports have been modelled as having no rotational restraint, when in the real-world this is not possible. Whereas, whilst the full fixed supports at the bases of the piers are modelled as being restrained in all degrees of freedom, in reality these may have some flexibility.

Based on site measurements, the depth of the slab is 0.6 m and the columns are modelled as 2.25 m tall with a 3 m × 1 m cross-section. To get the modal frequency of the FE model to match the value from the day of the modal test (5.54 Hz), it was found that the corresponding E value was 28.43 GPa. The air temperature recorded during the modal testing period varied between 9.1 °C and 15.9 °C. The mode shape predicted by the FE model is shown in Fig. 3(b), and this matches quite well with the experimentally measured mode shape shown in Fig. 2(d).

4.2.2. Long-term dataset of natural frequency and air temperature measurements

As described above, long-term data of bridge natural frequency and air temperature was collected in order to allow the diurnal and seasonal variation in bridge first natural frequency against air temperatures to be observed.

(a) (b)

Fig. 4. Photographs showing (a) Multifunction Extended Life acceleration logger, and (b) type of weatherproof enclosure used to secure the logger onto bridge.

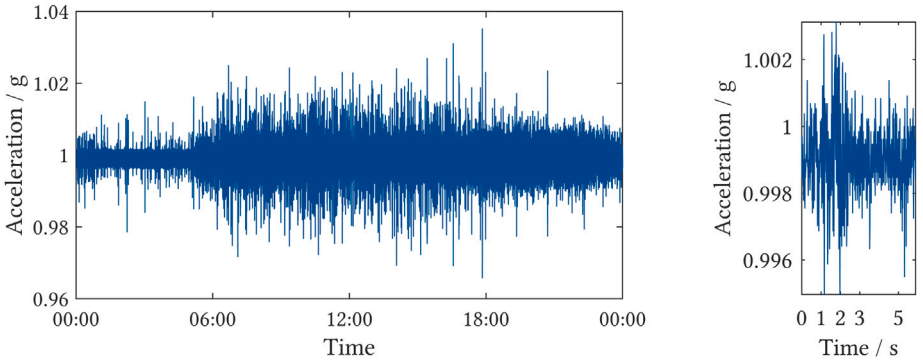

(a) (b)

Fig. 5. Plots of raw acceleration data for both: (a) a 24 h window and (b) a single vehicle crossing event.

Bridge natural frequency data collection

This long-term bridge natural frequency dataset was recently collected by researchers at Queen's University Belfast. Triaxial acceleration was recorded at 128 Hz using a Multifunction Extended Life acceleration logger from Gulf Coast Data Concepts, LLC. The readings were timestamped using a real-time clock chip and recorded onto an onboard micro-SD card. The logger is powered using 2 D-cell batteries, which give a run-time of up to 60 days of continuous recording.

The logger is pictured in Fig. 4(a) and shows both the weather-sealed case and the internal circuitry. A larger weather-sealed enclosure was secured onto the bridge at the quarter-span point to house the logger. Fig. 4(b) shows an example of this enclosure with the logger in place; the blue foam inserts in the enclosure ensured the logger was aligned consistently after being replaced when changing batteries or the micro-SD card. The quarter-span point was used for the long-term monitoring as a modal test carried out on the bridge before installation showed that the acceleration data from this point gave a high degree of modal energy to track the mode, and also this was a logistically convenient location to install the enclosure.

As an example of the acceleration signals recorded, Fig. 5(a) shows the raw acceleration data over a 24 h window; it can be noted that there is a higher amplitude and variance during the 'daytime' hours, i.e. 06:00–21:00, due to the higher number of vehicle crossings. Fig. 5(b) shows the typical acceleration waveform due to a single vehicle crossing. In particular, the free decay after the vehicle leaves the bridge can be seen.

To extract the frequencies from the long-term bridge acceleration measurements, the data was first binned into hourly windows, which were processed using a covariance-driven stochastic subspace identification (SSI) algorithm [23,24]. The full two years and three months covered by the natural frequency dataset are plotted in Fig. 6(a) with air temperature and frequency plotted against the left and right y-axes respectively.

Frequency data

Looking at just the frequency data in the first instance, the annual seasonality of the frequency data in the plot can be observed. Fig. 6(b) presents a single week of frequency data starting from 2019-06-01 in which the diurnal trends can be seen.

It is apparent from the time-series in Fig. 6 that: (1) there are a number of outliers in the frequency data below 5.4 Hz and above 6.0 Hz, and (2) there are periods of missing values with varying lengths. The longer periods of missing values occur whenever the

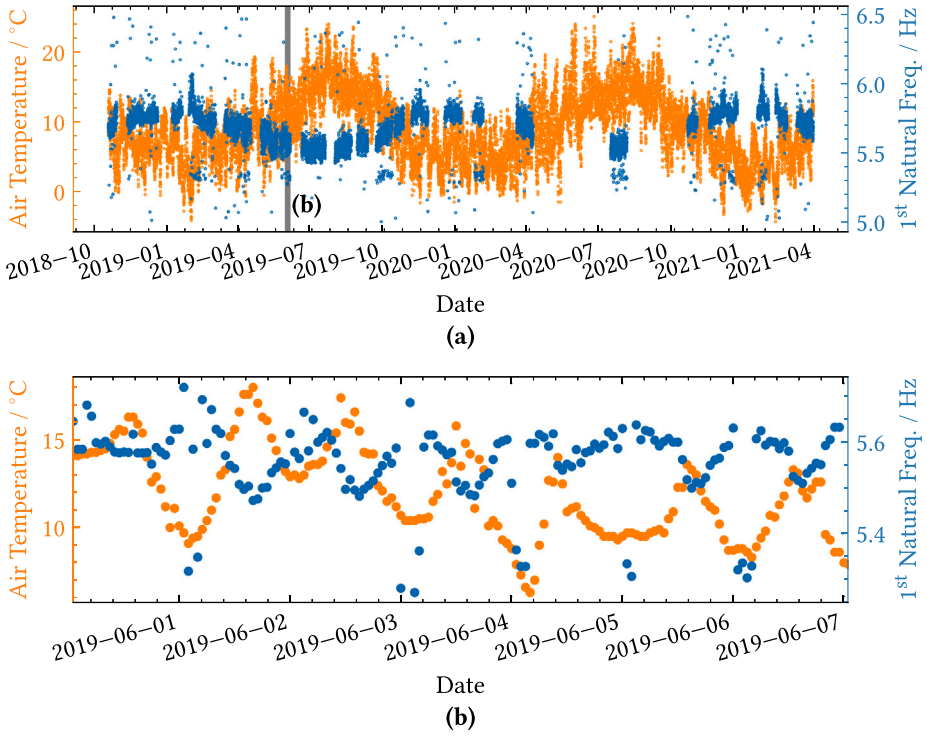

Fig. 6. Plot of raw first natural frequency values returned from the stochastic subspace identification algorithm and air temperature data for: (a) the full duration of the dataset and (b) a single week (indicated by the grey shaded region). (For interpretation of the references to colour in this figure legend, the reader is referred to the web version of this article.)

logger's batteries were depleted, before being replaced. The large gaps in 2020 were due to the COVID-19 regulations in Northern Ireland preventing any site visits. Due to the covariance-driven SSI method used, not every hour window returns a frequency as SSI algorithm screens out periods with low energy in the signal. However, in some windows, particularly at night when there are lower traffic volumes, the SSI algorithm returns anomalous frequency values as there was not enough external excitation to the structure to precisely obtain the modal frequency. The corresponding pre-processing steps to rectify these issues, (1) and (2), are described in Section 4.2.3.

Air temperature data

The air temperature measurements used are taken from the UK's Met Office Integrated Data Archive System (MIDAS) data collection [25], which is available under the Open Government Licence. The closest weather station in the MIDAS data collection with hourly data available was located approximately 9 km away to the north-west of the bridge location. The air temperature data from this station covering the same period as the frequency measurements is plotted in Fig. 6. The annual cycles in air temperature are apparent in the two year plot (Fig. 6(a)). In Fig. 6(b), the diurnal temperature cycles are clearly visible. In both these plots, the negative correlation between air temperature and frequency can be also be observed.

4.2.3. Time-series data model

Data models that can predict bridge natural frequencies based on temperature have been proposed previously, such as [21]. Various data modelling approaches have been proposed for long-term approaches, such as artificial neural networks [26] and auto-regressive with exogenous inputs models [21].

In this work, an autoregressive distributed lag (ARDL) model [27,28] is fitted to capture the relationship between the air temperature and bridge natural frequency data. Specifically, the ARDL model has the form:

$$y[t] = \beta_0 + \beta_1 y[t-1] + \cdots + \beta_p y[t-p] + \alpha_0 x[t] + \cdots \alpha_q x[t-q] + \epsilon[t], \tag{8}$$

where the independent variable, $x[t]$, is air temperature, the dependent variable, $y[t]$ is bridge natural frequency, and $\epsilon[t]$ represents a white noise error. This model can capture short-run effects by including lagged terms of the air temperature, e.g. α_1 represents the effect of a unit change in air temperature one hour ago on the current bridge natural frequency. The lagged values of the bridge natural frequency help to model the effect of 'memory' or 'inertia' in the system, i.e. a large, positive value for β_1 would indicate that if the bridge natural frequency was high one hour ago then the bridge natural frequency is likely high now as well. In order to

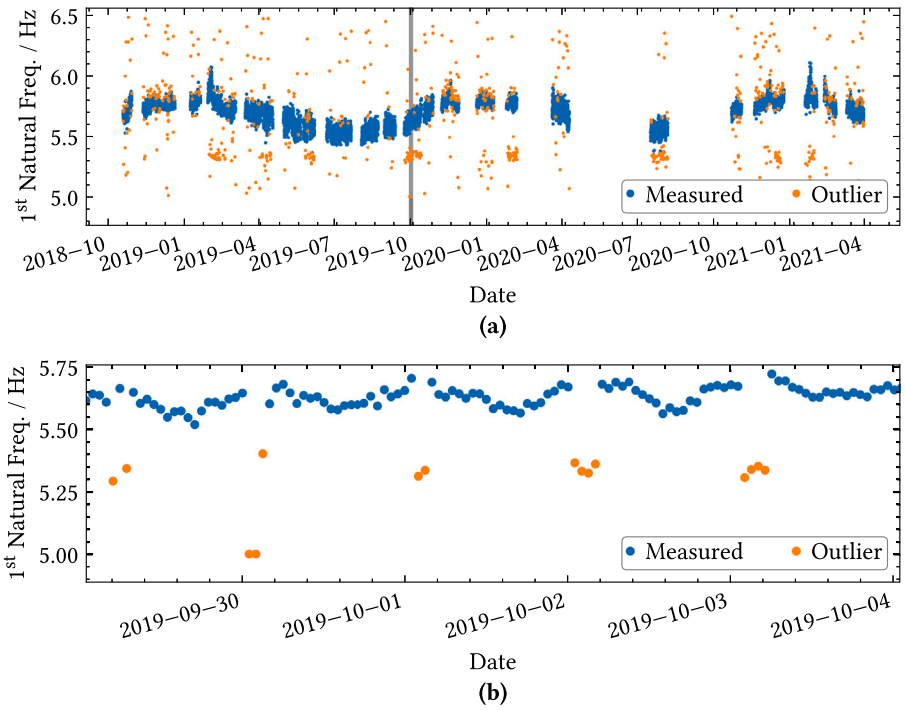

Fig. 7. Plots showing the outlier detection and interpolation pre-processing steps applied to the natural frequency data for: (a) the full duration of the data set, and (b) 5 days worth of data (indicated by the grey shaded region). (For interpretation of the references to colour in this figure legend, the reader is referred to the web version of this article.)

fit this ARDL model to our data, it is essential to carefully optimise the choice of these lag lengths, denoted p and q, using a model selection technique, in this case by holdout validation, which is described subsequently.

A key assumption of this data model is that the relationship between air temperature (x) and bridge natural frequency (y) is linear. However, incorporating lags of both the air temperature and bridge natural frequency allows the model to better capture the dynamic relationship between these variables, i.e. that bridge natural frequency does not change instantaneously with varying air temperature, but instead may depend on past temperatures and its own past values.

Data pre-processing

As explained above, there are some measurement periods, often at night, when there are not enough vehicles crossing the bridge to get reliable frequencies, but the SSI algorithm does not always screen out these windows. The resulting small number of anomalous points are removed using a Hampel filter [29] which employs the Hampel identifier (an outlier robust estimator of the 3-sigma rule in statistics) over a sliding window to identify and remove these anomalous points. Observations lying outside a rolling interval of $\tilde{x}[t] \pm h \times (1.4825 \times \text{MAD}[t])$ are outliers, where $\tilde{x}$ is the median of window, and MAD is the median absolute deviation of the window. The consistency constant, 1.4826, ensures that $1.4826 \times \text{MAD}$ is an outlier robust estimator of the standard deviation for normally distributed data. The window length for the filter was set at 24 h and the outlier threshold, $h = 3.5$, was used as recommended by other researchers [30].

As shown in Fig. 7(a), out of a total of 21 434 data points, this filter removes 839 (3.84 %) of the data points as outliers, i.e. the points above and below the main band of frequencies. Fig. 7(b) presents five days of data, and as it is reasonable to assume the bridge natural frequency evolves smoothly, indicates that some likely outliers remain such as the two points around 2019-09-30. However, it was found that further decreases of the threshold or window length, resulted in more clearly false positives being removed.

The distribution of outliers detected throughout the hours of the day are plotted in Fig. 8, to check that the outliers are being removed mostly at night, when it is to be expected that the lower traffic volume would lead to more erroneous frequencies from the SSI algorithm. It is clear that the majority of the outliers have been detected during the night as would be expected, only 10.1 % of the outliers occurred during the 'day time' hours of 07:00–19:59, compared to 89.9 % during the 'night time' hours of 20:00–06:59.

Time-series data model fitting

The pre-processed long-term air temperature and frequency dataset were split by partitioning the data into a 70 % training set and a 30 % testing set, as shown in Fig. 9, where the vertical dashed line indicates the partition boundary. This split ensured that the testing set contained at least a full cycle of the annual temperature cycle. Furthermore, as the fitting of the ARDL model requires

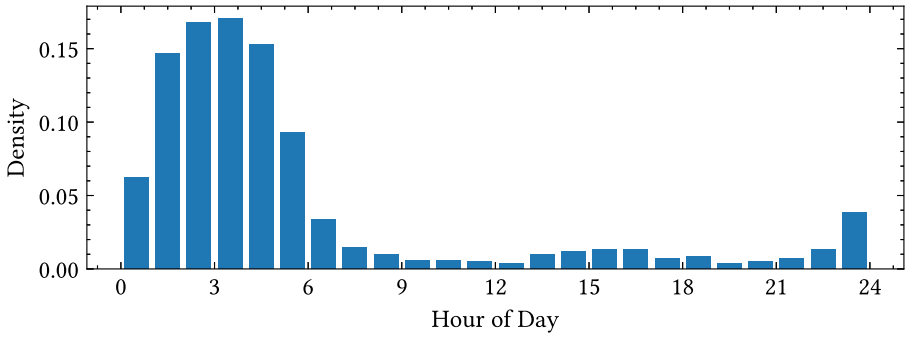

Fig. 8. Histogram plotting the density of outliers detected for each hour of the day.

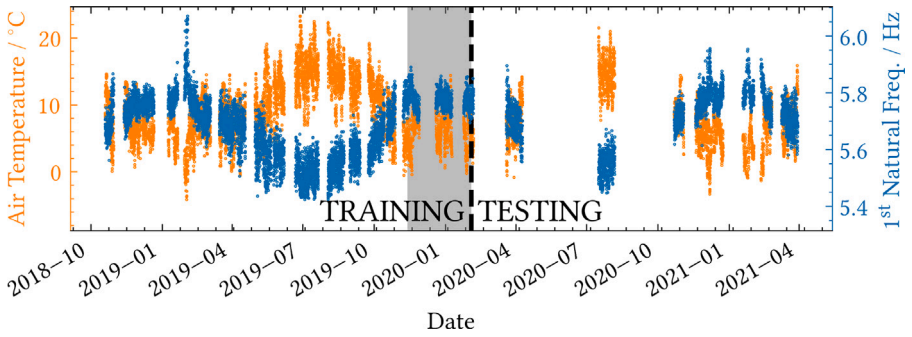

Fig. 9. Full pre-processed dataset of bridge natural frequency and air temperature with the training and test set split annotated. Grey shaded region indicates validation set used to select model hyper-parameters. (For interpretation of the references to colour in this figure legend, the reader is referred to the web version of this article.)

selecting orders for the auto-regressive and distributed lag components, a further hold out of 20 % from the end of the training set was made to form a validation set.

The orders, p, and q for the auto-regressive and distributed lag components are first estimated by training the ARDL model for varying orders up to maximum lags of 9 h. Using the held-out set, it was established that ($p = 4, q = 2$) gave the smallest root-mean-square error (RMSE) (0.472 Hz). Using these orders, the ARDL model was then trained using the full training set and the RMSE was computed as 0.053 Hz and 0.050 Hz for predictions using the training and test set respectively. The predicted frequency data is plotted in Fig. 10(a), where it can be observed that the model is achieving a good recreation of the annual seasonal cycles of frequency. Figs. 10(b) and 10(c) show one week's worth of predicted frequencies from both the training and testing set. These plots show that the model is capable of approximating the diurnal variation in frequency as well, and the similar performance in both the training and testing data would suggest no over-fitting has occurred.

In addition to visually assessing the fit of the predictions in Fig. 10, the distribution of the residuals of the model can be examined in Fig. 11, where it can be noted that the residuals from the training and testing set are very similar, which is an important metric in ascertaining the accuracy of the time-series data model. Specifically, Fig. 11(a) shows the histogram of residuals, and shows an approximately normal distribution with a mean of zero for both the training and test data. Fig. 11(b) shows that the residual frequency does not vary significantly with predicted frequency or between training and testing sets. Finally, Fig. 11(c), plots the residual at each time step versus the residual at the previous time step. This allows the presence of serial correlation to be observed. In this case the positive serial correlation means that a prediction with a positive error will likely be part of run of positive errors (or similarly for negative errors).

4.2.4. Transformation from bridge natural frequency to Young's modulus values

A transformation was then fitted to allow the time-series data model to predict E values for reinforced concrete for a given air temperature time-series. Firstly, the FE model was tuned by taking a series of first natural frequencies between the minimum and maximum natural frequencies predicted in the dataset. For each natural frequency, the FE model's stiffness, E, was varied such that the natural frequency matched that obtained from the eigenfrequency analysis.

The resulting Young's modulus values are plotted in Fig. 12. In this instance, it was found that a linear fit, $E = 11.34\, f_1 - 32.1$ GPa, was a very good approximation ($R^2 > 0.99$); however, it is acknowledged that this choice of function will depend on the particular structure under test and its structural properties. This linear transform is applied to the previously shown predicted frequency data to obtain the E values to apply to our FE model.

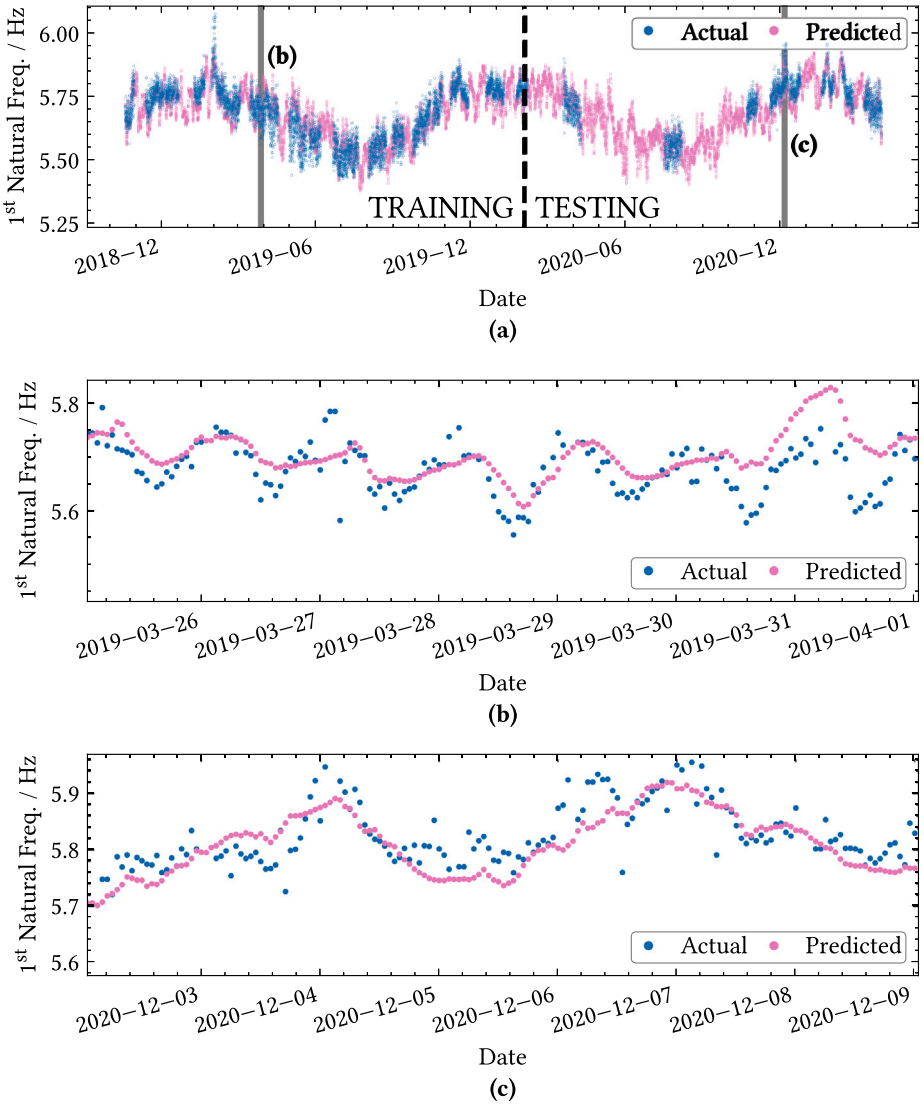

Fig. 10. Predicted bridge first natural frequency for (a) full duration of long-term measurement dataset, (b) one week window in training set, and (c) one week window in test set.

For illustration, the fitted ARDL model and transformation can be applied to 51 years worth of air temperature data from Aldergrove Airport, Northern Ireland [25]. The resulting predicted reinforced concrete E value time-series are plotted in Fig. 13(a), where the annual cycles due to seasonal temperature variation can be observed. Figs. 13(b) and 13(c) plot two years, and one week's, worth of air temperatures and predicted E values, respectively, to allow the variation over short time frames due to diurnal temperature variations to be observed.

Thus, we now have a method of getting an E value time-series for reinforced concrete for a given temperature time-series with a reasonable level of variation due to seasonal and diurnal temperature changes, which can be applied to the single span bridge model shown in Fig. 1.

4.3. Stochastic vehicle arrival model

Modelling traffic flows is well established in civil engineering with the most fundamental model being that of a Poisson distribution [31–33], which models the probability of the number of events, n, occurring in a given interval with an average occurrence rate, λ, as:

$$P(n) = \frac{\lambda^n}{n!} e^{-\lambda}. \tag{9}$$

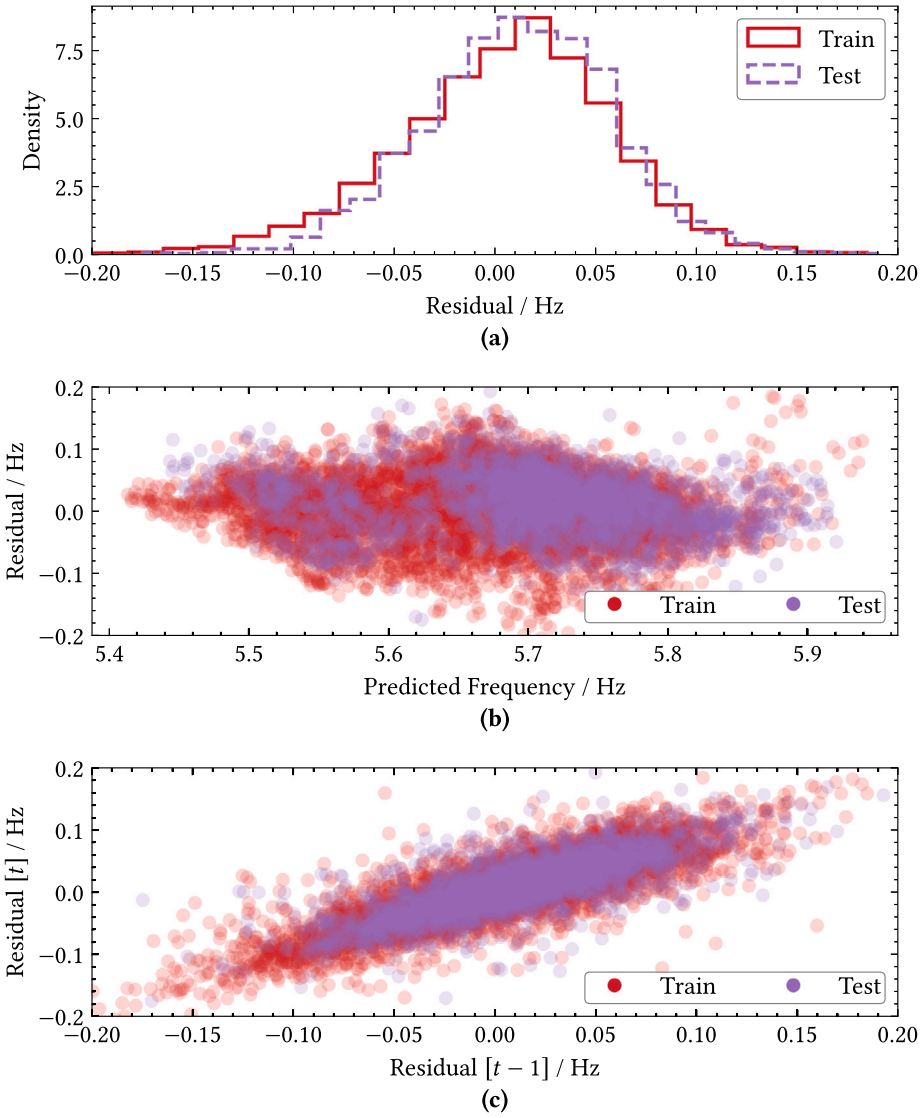

Fig. 11. Diagnostic plots of (a) histograms of residuals, (b) residual versus prediction, and (c) serial correlation plot.

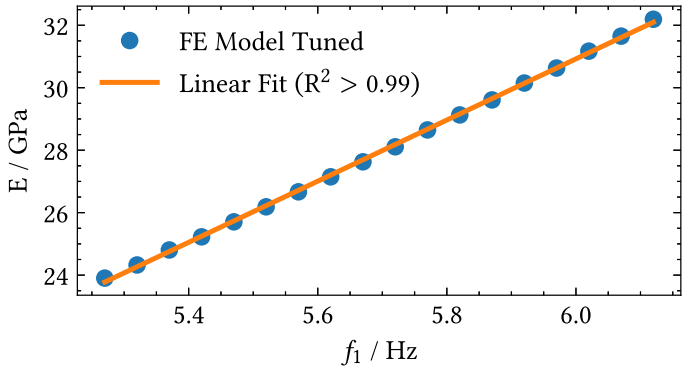

Fig. 12. Plot of tuned FE model Young's modulus values, E, versus first natural frequency, f_1.

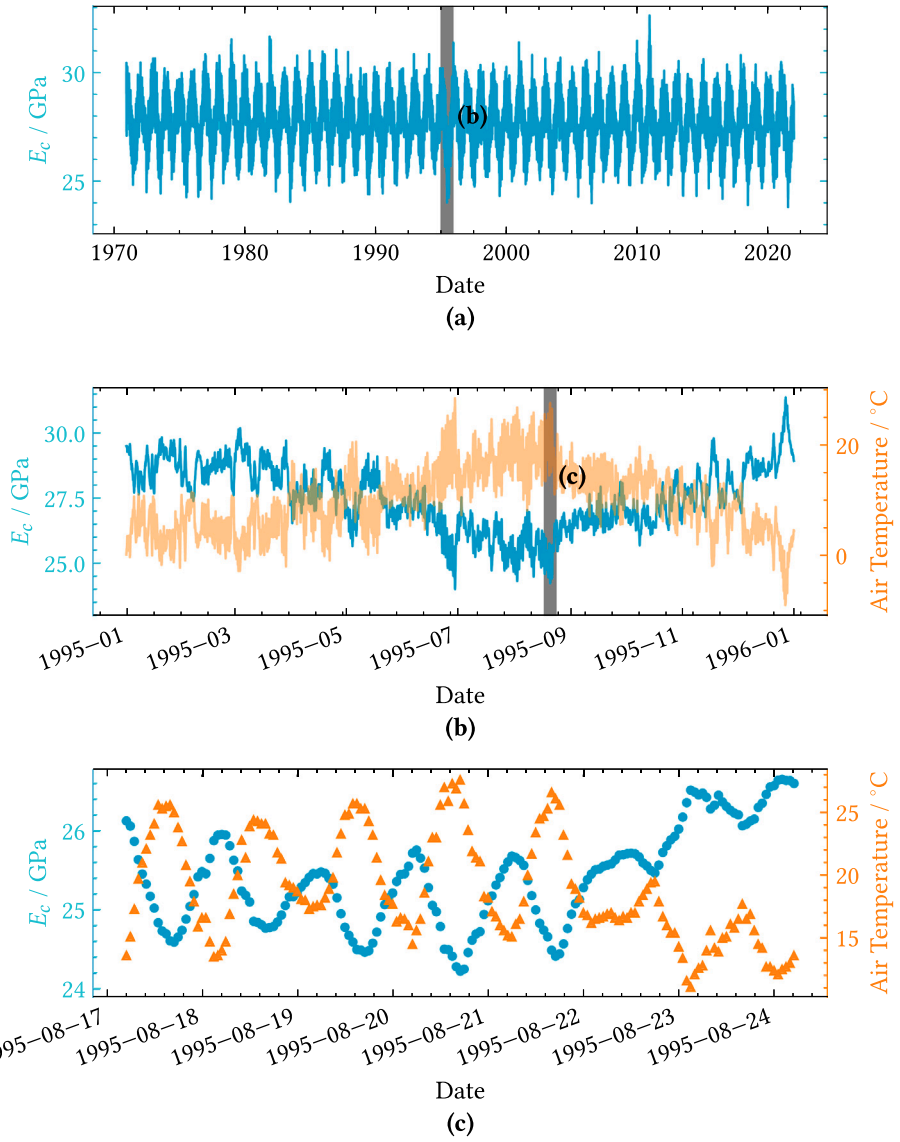

Fig. 13. Predicted bridge Young's modulus values for (a) 51 years spanning 1970–2021, (b) two years for 1994–1995, and (c) one week from August 1995.

In this work, we use the Poisson distribution with the value of λ varying over time to randomly generate the sequence of vehicle arrivals at the bridge. A limitation of the model is that this only generates temporal distributions of vehicles for free-flow traffic conditions.

Using data from a WIM dataset [34], we justify the application of a Poisson distribution using data for a single site to obtain the hourly vehicle counts for a particular day-of-the-week and hour-of-the-day, which, in this case, was Fridays between 07:00:00 and 07:59:59. The histogram of these hourly counts of 2-axle vehicles is shown in Fig. 14(a). The theoretical Poisson distribution is obtained by setting the average rate of occurrences, λ, to the mean value of the histogram ($77.98\,\mathrm{h}^{-1}$). Similar histograms and Poisson distributions were plotted for 5-axle ($\lambda = 69.18\,\mathrm{h}^{-1}$), and 6-axle ($\lambda = 31.78\,\mathrm{h}^{-1}$) vehicle counts in Figs. 14(c) and 14(e), respectively. In all of these figures, a good correspondence can be observed between the WIM data and the Poisson distributions. To further increase the temporal granularity of the vehicle arrivals, the minute-level vehicle counts can also be modelled as demonstrated by the plots in Figs. 14(b), 14(d) and 14(f). At this level, the Poisson distribution provides an even better approximation of the observed WIM data.

To generate a random sequence of vehicle arrivals, this only requires the average rate of vehicles for a particular axle count, λ, which can be randomly sampled from the WIM dataset. For each minute, a random sample is then taken from a Poisson distribution with value of λ for each vehicle class. To demonstrate the result of this process, a random sequence of vehicle arrivals for a Friday between 07:00 and 08:00 is shown in Fig. 15(a). Similarly, a random sequence of vehicle arrivals for a Friday between 15:00–16:00

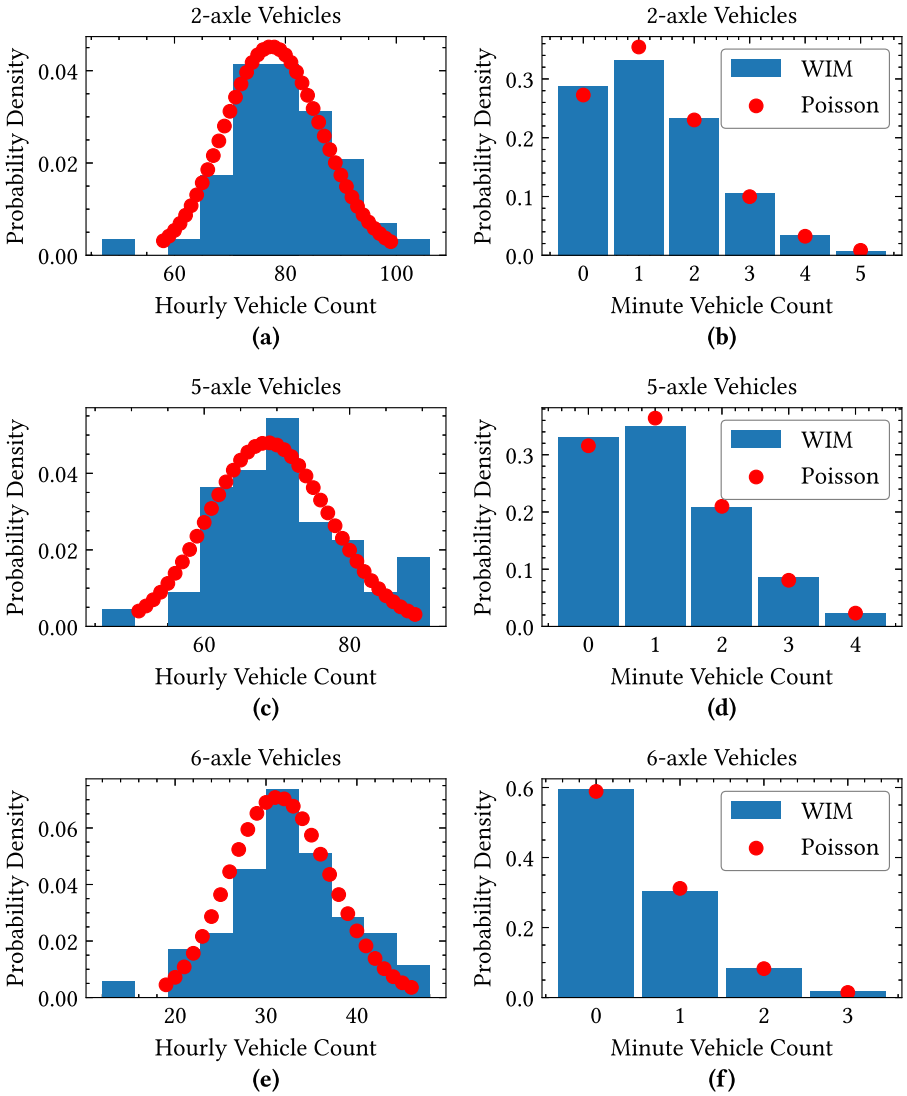

Fig. 14. Histograms and fitted Poisson distributions for (a) hourly 2-axle vehicle counts, (b) minute-level 2-axle vehicle counts, (c) hourly five-axle vehicle counts, (d) minute-level five-axle vehicle counts, (e) hourly six-axle vehicle counts, and (f) minute-level six-axle vehicle counts.

and 22:00–23:00 are plotted in Figs. 15(b) and 15(c) showing that the model can recreate the differences in total volumes and composition of traffic at different times of the day. However, it should be noted that a limitation of this approach is that it only models free-flow traffic arrivals.

The process to then generate axle weights and spacings for each of the vehicle arrivals is illustrated using the first six vehicles in Fig. 15(a), namely, a 5-axle vehicle, two 2-axle vehicles, a 6-axle vehicle, a 5-axle vehicle, and a 3-axle vehicle. This consists of taking a random sample with replacement from the subset of the WIM dataset that has the required axle count. The resulting ensembles of point forces obtained from this sampling for these first six vehicles are shown in Fig. 16.

A traffic profile can then be generated by first randomly sampling an average rate of arrival of each vehicle by axle count for every hour, and to ensure the rate of arrivals varies smoothly, these are interpolated across the minutes in each hour period. A random draw is then made from the Poisson distribution with the corresponding λ for each minute and axle count. Finally, axle weights and spacings are obtained by taking random samples from the WIM dataset with replacement, i.e. a particular 'vehicle' from the WIM dataset can be sampled multiple times, just like randomly selecting tokens from a bag and replacing them after each draw.

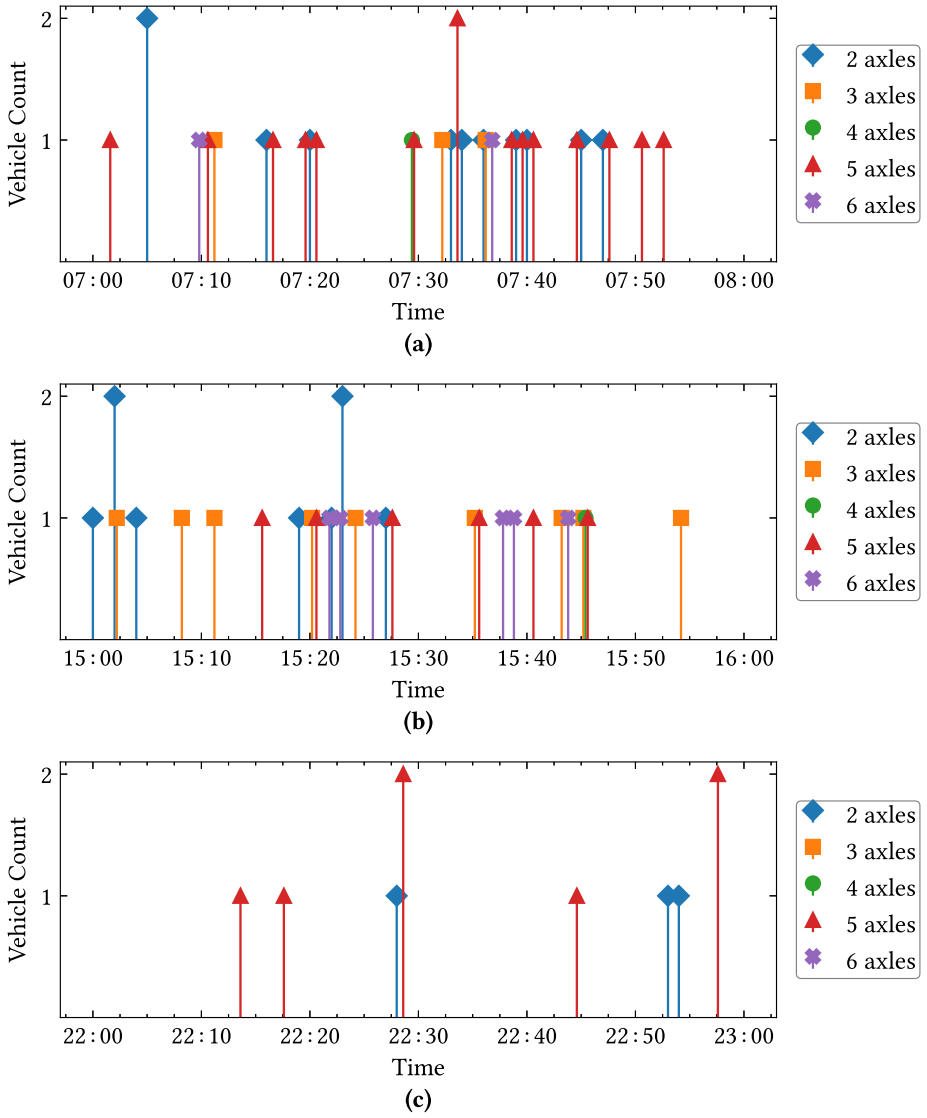

Fig. 15. Random generated sequences of vehicle arrivals for (a) 07:00–08:00, (b) 15:00–16:00, and (c) 22:00–23:00.

5. Sampling methods based on expected traffic volumes for resource-constrained environments

To demonstrate the potential for leveraging knowledge of expected traffic volumes for long-term bridge monitoring, three sampling methods have been proposed, which allow the system to elect when to be 'on', or to conserve power and go into a low-power 'sleep' state. For simplicity, we assume that each sampling method will elect the state of the system for each hour of the day. As an example of a typical resource-constraint, we will consider a system with a limited energy budget, which we simulate by restricting the 'on' time of the system. Therefore, each sampling algorithm was tuned such that it would not exceed the chosen 'on' time limit, i.e. it would not oversample and exhaust the systems energy budget for a given time-period.

This limit was chosen as 12.5 % of the hours in each month, as this represents almost an order of magnitude less 'on' time, whilst conveniently dividing the 24 h of a day into a whole number, thereby preventing the peak traffic-volume hours method described below being penalised. As the maximum rotation amplitude data set obtained using these sampling methods will be smaller than the total population, it is unfair to compare its performance against a damage detector utilising the full population, cf. standard error of the mean, $\mathrm{SEM}_N = s/N^{\frac{1}{2}}$, where s is the standard deviation of the sample, and N, the sample size. Hence, a wholly random hourly sampling approach is presented to serve as a fair comparison for the rest of the algorithms and then compared with two sampling methods based on expected traffic volumes.

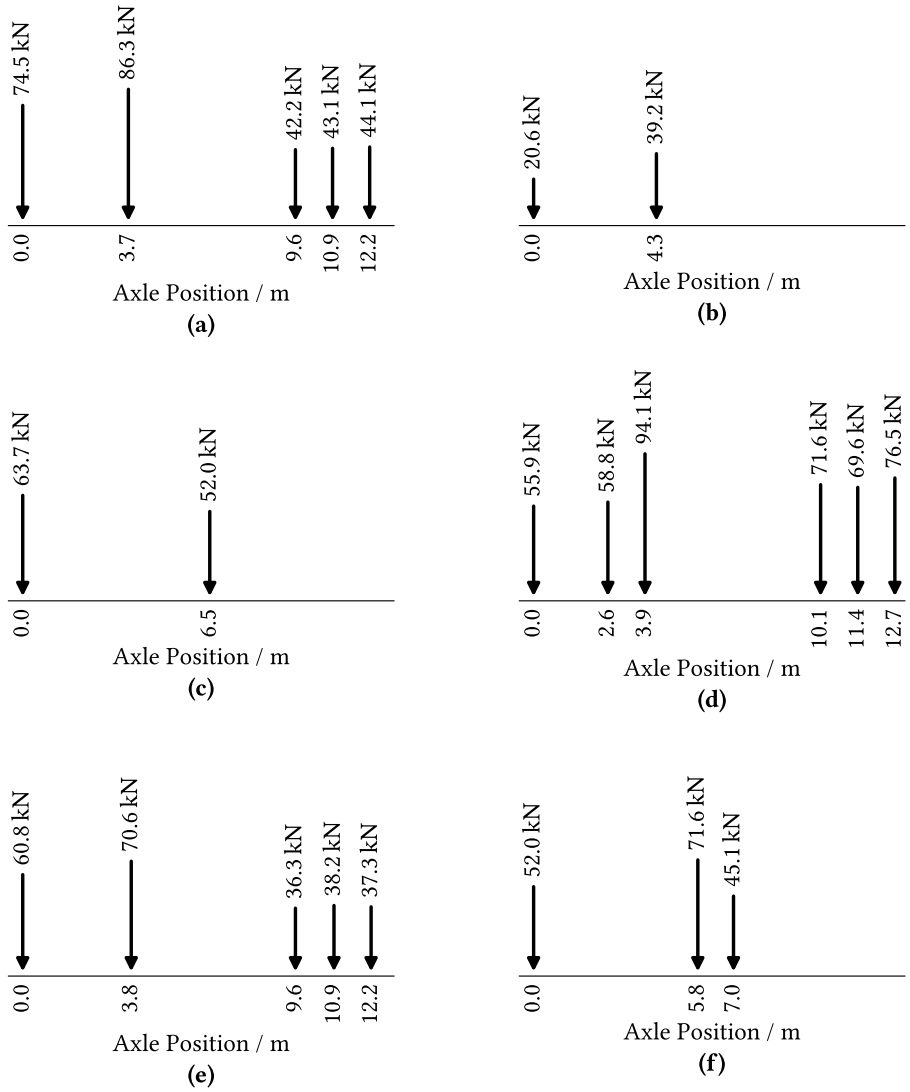

Fig. 16. Randomly selected axle configurations (weights and spacings) for 6 vehicles.

5.1. Random hourly sampling windows

The first method described serves as a benchmark for the rest of the algorithms described herein. This naive sampling approach consists simply of a random election process carried out at the start of each hour, wherein the system decides whether or not it will be in the 'on' state for the next hour, $h \in \{0, \ldots, 23\}$, at random. The state election is based on the following inequality:

$$\text{state}\,(h) = \begin{cases} \text{'on'}, & \text{if } X \leq k_t, \quad X \sim U(0,1), \\ \text{'off'}, & \text{otherwise.} \end{cases} \tag{10}$$

The threshold, k_{on}, can be set as the ratio of the time that we desire the system to be 'on', Time_{on} and the total time, $\left(\text{Time}_{\text{on}} + \text{Time}_{\text{off}}\right)$, i.e.:

$$k_{\text{on}} \approx \frac{\text{Time}_{\text{on}}}{\text{Time}_{\text{on}} + \text{Time}_{\text{off}}}. \tag{11}$$

5.2. Peak traffic volume hours sampling

If the target is to optimise the number of vehicle crossings captured, it would seem reasonable to focus the sensor system's limited resources on only the subset of hours of the day that have the highest traffic counts. In advance of the monitoring, a traffic survey

could be conducted to establish the temporal distribution of traffic on the bridge under test, or it would be trivial to incorporate some traffic counting functionality into the sensor system. This sampling algorithm can be described as follows: firstly, let the set, $C = \{c_0, \dots, c_{23}\}$, be the aggregated average counts, or volumes, of traffic in each hour of the day. The subset of hours, S, for which we want the system to be 'on', can then be obtained as the n largest expected traffic volume hours, where k_{on} again represents the desired proportion of time to have the system 'on', i.e.:

$$S = \left\{ h_0, \dots, h_n \mid c_{h_0} \geq \cdots \geq c_{h_n} \geq c_i \forall i \notin S \right\}, \quad n = \lfloor 24\, k_{\text{on}} \rfloor. \tag{12}$$

The state election for each hour, h, can then simply be determined as follows:

$$\text{state}\,(h) = \begin{cases} \text{'on'}, & \text{if } h \in S, \\ \text{'off'}, & \text{otherwise.} \end{cases} \tag{13}$$

5.3. Traffic volume probability proportional sampling

Instead of restricting the sampling to only the subset of hours which had the largest traffic counts, it may be advantageous to allow sampling in any hour. However, to expend the system's limited resources more efficiently, it would seem sensible to make the system more likely to be 'on' during hours which are more likely to have higher numbers of vehicle crossing. To estimate the likelihood of a given vehicle crossing occurring in a given hour, h, the aggregated traffic counts, C, can be used, i.e.:

$$P\,(h) = \frac{c_h}{\Sigma C}$$

The state election can then be determined by:

$$\text{state}\,(h) = \begin{cases} \text{'on'}, & \text{if } X \leq k_v P\,(h), \quad X \sim U(0,1), \\ \text{'off'}, & \text{otherwise,} \end{cases} \tag{14}$$

where k_v is a coefficient that can be varied to ensure that the system is 'on' for the desired proportion of the time, k_{on}.

As the state election is carried out continually for each hour, $h \in \{0, \dots, 23\}$, a reliable estimation of the value for k_v can be determined through simulation by running the state election process for a large number of hours with a range of k_v values and recording the proportion of 'on' hours. Repeating this procedure multiple times allows a confidence interval for the 'on' time to be obtained for increasing values of k_v, from which an appropriate value can be chosen depending on the target 'on' time.

6. Numerical simulations and results

To assess the performance of the sampling methods set out in the previous section (Section 5), 60 years worth of long-term bridge rotation data was generated using the environmentally capable FE model. The bridge modelled used is the single-span bridge shown in Fig. 1. The E values to apply to the model at each time-step are obtained by applying the ARDL model and transformation developed in Sections 4.2.3 and 4.2.4 to 60 year's of air temperature data from Aldergrove Airport, Northern Ireland [25]. To simulate representative loading the stochastic vehicle arrival model, described in Section 4.3 was used.

In previous work [15], these long-term numerical simulations consisted of: (a) running a dynamic solve for each vehicle crossing, (b) applying an empirically-tuned sensor noise model based on Fourier-transformed surrogates, (c) low-pass filtering to obtain the static rotation component, and (d) extracting the maximum rotation amplitude via a peak prominence algorithm to obtain our damage-sensitive feature, A_d.

Due to the very large number of simulations needed, it was determined that using the environmentally capable FE model with a full dynamic solver was not a sensible approach as results could not be returned in a reasonable time-frame. For this work, however, we did not require the exact dynamic response, but needed to capture the variation in the measured maximum static rotation amplitude due to both dynamics and the signal processing stage. Thus, to speed up the simulations, static solves, i.e. $\boldsymbol{F} = \mathbf{K}\boldsymbol{x}$, were carried out to obtain the rotation amplitudes used as the feature for our EMD-based damage detection approach, with a random multiplicative error term, ε, added to allow for any variation that would arise from the vehicle dynamics or signal processing, such that:

$$A_d = \varepsilon \times A_s,$$

where A_s is the rotation amplitude (peak prominences) obtained with the static solver. The multiplicative error model avoids the heteroscedasticity over varying gross vehicle weight/rotation amplitude that occurs with an additive error model.

The distribution for this multiplicative error, ε, was sampled by running the same 1000 random vehicles through both the full dynamic solver and signal processing (A_d), and the static solver and peak amplitude (A_s). The multiplicative error between these was calculated and plotted for the LHS rotations in Fig. 17, giving errors with a mean, $\mu = 1.02$, and standard deviation, $\sigma = 0.0277$.

The one-sample Kolmogorov–Smirnov (K–S) test was used to check the goodness of fit between the simulated error distribution and a fitted parametric distribution with a significance, $\alpha = 0.05$; where the null hypothesis of the test is that the distributions are identical with the alternative hypothesis being that they are non-identical. First, a normal distribution was fitted to the simulated errors, which had mean, $\mu = 1.02$, and standard deviation, $\sigma = 0.0276$. From Fig. 17, it can be seen that the normal distribution exaggerates the tails of the error distribution, consequently leading to a decrease in probability density around the mean. This lack of fit is confirmed by the K-S test ($p < 0.001$), indicating that the null hypothesis can be rejected, i.e. the simulated error distribution and the fitted normal distribution was non-identical.

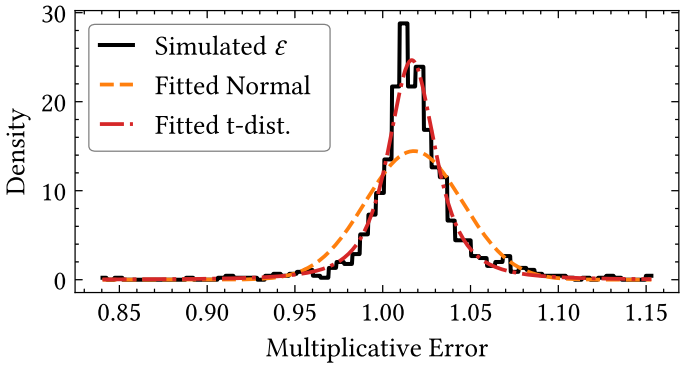

Fig. 17. Plot of multiplicative error, ε, distribution from dynamic and static simulations and fitted normal and t-distributions.

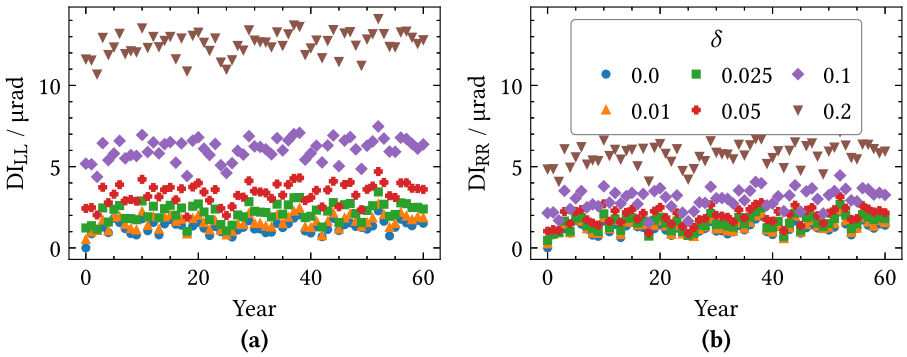

Fig. 18. Scatter plots of 60 years for six crack damage levels of: (a) DI_{LL} and (b) DI_{RR}.

A Student's t-distribution (Fig. 17) was then fitted to the simulated errors as the degrees of freedom parameter allows the mass of the distribution to be more concentrated around the mean (as in the simulated error distribution). The parameters of the fitted distribution were found to have $\nu = 2.21$ degrees of freedom, and a mean, $\mu = 1.02$, and standard deviation, $\sigma = 0.0468$. The K-S test ($p = 0.328$) showed that this fitted t-distribution was identical to the simulated error distribution to a 5 % significance; therefore, in the remaining simulations, we will use random multiplicative error values from t-distributions (fitted in the manner described above) to introduce an appropriate level of variation to our simulated results.

6.1. Numerical simulation results with no sampling

The long-term numerical simulations were carried out for the single-span bridge described in Section 4.1 with localised damage at the third-span location from the LHS.

For illustration, the bridge was first subjected to six damage levels, $\delta \in \{0.0, 0.01, 0.025, 0.05, 0.1, 0.2\}$. The mean (and standard deviation (SD)) of the number of vehicle events per annum was 100 278 (437.2). The results of applying the EMD-based metrics, DI_{LL} and DI_{RR}, to these 60-year sets of rotation amplitudes are plotted in Fig. 18. Specifically, in Fig. 18(a), it can be seen that for the LHS end-of-span, the increases due to increasing damage levels are more pronounced than the corresponding RHS results (Fig. 18(b)). In these results, it can also be observed that both a short-term variation and a longer-term trend exist in the damage detection metrics for all damage levels.

The damage detection capability is assessed by observing which damage levels have prediction intervals (PIs) for the damage indicator, DI, that are disjoint to the corresponding PI of the 'healthy' ($\delta = 0.0$) case; this means that with PIs, $H = [h_a, h_b]$, for the 'healthy' case, and $D = [d_a, d_b]$, for the damaged case, these would be disjoint when $H \cap D = \varnothing$. Assuming the system was originally in the 'healthy' state, this means that for a given confidence level, in this case 95 %, observations from a future damaged state would appear as outliers, thus being readily detected by outlier analysis. This approach was adopted as it was felt to offer a conservative estimate of the level of damage which would likely be observable, whilst being a rather general result, i.e. this does not depend on a particular choice of outlier detection algorithm or other such implementation-specific details.

Kernel density estimation is used to obtain a non-parametric estimator, $\widehat{f}(x)$, for the probability density function (PDF) of the damage detection metric values for each damage level. The PI can then be obtained from the estimator of the inverse cumulative

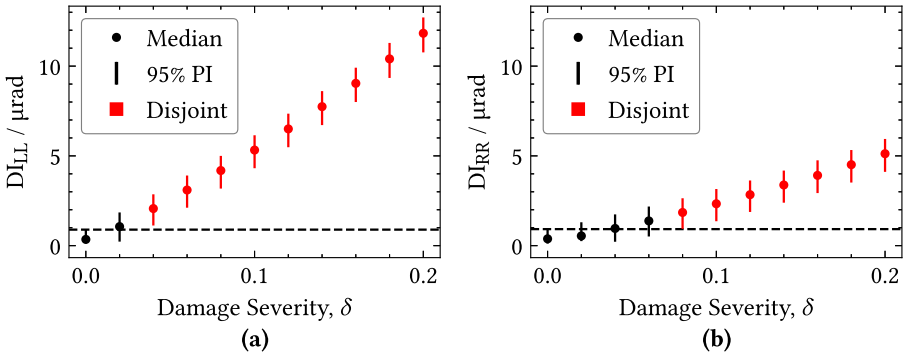

Fig. 19. Plots of 95 % PIs and medians for EMD-based damage indicators, DI_{LL} and DI_{RR}, with no sampling over varying damage severity of: (a) DI_{LL} and (b) DI_{RR}. Horizontal black dashed line indicates upper bound of PI for 'healthy' ($\delta = 0.0$) condition.

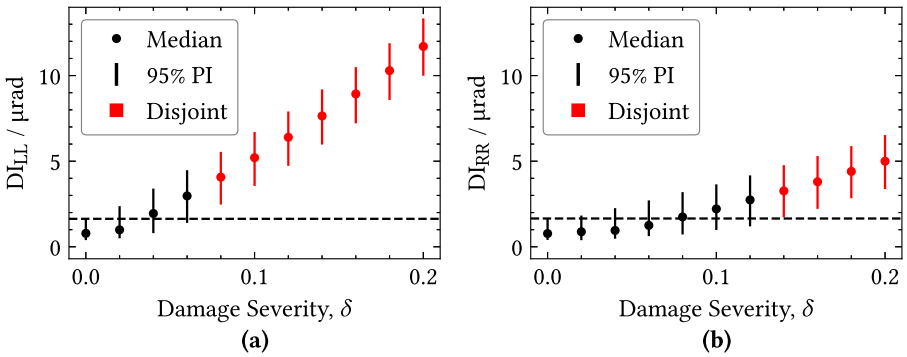

Fig. 20. Plots of 95 % PIs and medians for EMD-based damage indicators, DI_{LL} and DI_{RR}, with random hourly sampling over varying damage severity of: (a) DI_{LL} and (b) DI_{RR}. Horizontal black dashed line indicates upper bound of PI for 'healthy' ($\delta = 0.0$) condition.

distribution function, $\widehat{F}^{-1}(p) = x$, where $p \in [0, 1]$, such that, $\widehat{f}(x) = p$. Therefore, the 95 % PI is, $[\widehat{F}^{-1}(0.025), \widehat{F}^{-1}(0.975)]$, i.e. the interval bounding the central 95 % of the estimated PDF.

To more clearly observe the behaviour of these PIs with increasing damage severity, the numerical simulations were repeated for $0.0 \leq \delta \leq 0.2$ in 0.02 increments, and these PIs are plotted in Fig. 19. From Fig. 19(a), it can be seen that for the LHS end-of-span damage indicator, DI_{LL}, that damages of at least $\delta = 0.04$ would be observable; and for the RHS end-of-span damage indicator, DI_{RR}, in Fig. 19(b), it can be seen that, as expected, damage would likely only be observed from at least $\delta = 0.08$, due to the damage being closer to the opposite end of the span.

6.2. Numerical simulation results with sampling

This section shows the effect of applying the various sampling methods, described in the previous section, on the damage detection capability of our EMD-based damage detection approach. To ensure a reasonable comparison between these approaches, the proportion of 'on' hours in each month has been kept constant at 12.5 %. This ensures that any variation in the number of vehicle crossings captured, and the damage detection capability, can be related to the efficiency of the sampling method employed.

6.2.1. Randomly hourly sampling windows

After applying the random hourly sampling method, the mean (SD) of the number of vehicle events per annum was 12 531 (252.4). The 95 % PIs for the damage detection metrics, DI_{LL} and DI_{RR}, are plotted in Fig. 20. For the LHS end-of-span damage indicator, DI_{LL}, it can be seen that the minimum damage level detectable is at least $\delta = 0.08$. For the RHS end-of-span, this also shows reduced sensitivity to damage, with the minimum level of damage likely to be detected being $\delta = 0.14$.

6.2.2. Peak traffic volume hours-only sampling

After applying the peak traffic volume hours-only sampling, the mean (SD) of the number of vehicle events per annum was 19 341 (155.3). The 95 % PIs for the damage detection metrics, DI_{LL} and DI_{RR}, are plotted in Fig. 21. For the LHS end-of-span damage indicator, DI_{LL}, it can be seen that the minimum damage level detectable is at least $\delta = 0.06$; and the RHS end-of-span damage indicator, DI_{RR}, again shows reduced damage sensitivity, with the minimum levels of damage likely to be detected being $\delta = 0.10$.

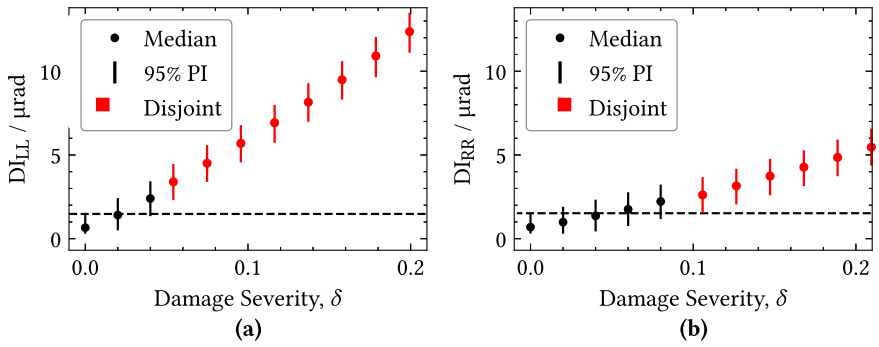

Fig. 21. Plots of 95 % PIs and medians for EMD-based damage indicators, DI_{LL} and DI_{RR}, with peak traffic volume hours only sampling over varying damage severity of: (a) DI_{LL} and (b) DI_{RR}. Horizontal black dashed line indicates upper bound of PI for 'healthy' ($\delta = 0.0$) condition.

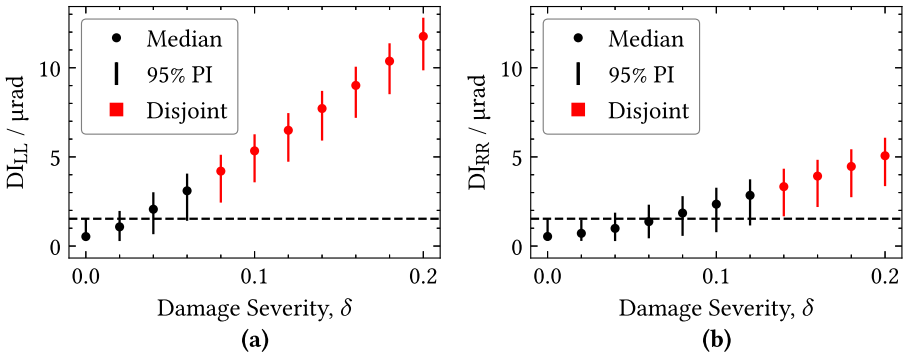

Fig. 22. Plots of 95 % PIs and medians for EMD-based damage indicators, DI_{LL} and DI_{RR}, with expected traffic volume proportional sampling over varying damage severity of: (a) DI_{LL} and (b) DI_{RR}. Horizontal black dashed line indicates upper bound of PI for 'healthy' ($\delta = 0.0$) condition.

Table 2
Summary of results for each sampling method showing mean number of vehicles crossings captured per year, N_{year}, and estimated minimum damage severity detectable using the rotation measured at the LHS end-of-span, δ_{LHS}, and the RHS end-of-span, δ_{RHS}.

Sampling method	T_{on}	N_{year}	δ_{LHS}	δ_{RHS}
No sampling	100.0 %	100 278	0.04	0.08
Peak traffic hours	12.5 %	19 341	0.06	0.10
Traffic volume prop.	12.5 %	15 304	0.08	0.14
Random hourly	12.5 %	12 531	0.08	0.14

6.2.3. Expected traffic volume proportional sampling

After applying the expected traffic volume proportional sampling, the mean (SD) of the number of vehicle events per annum was 15 304 (209.4). The 95 % PIs for the damage detection metrics, DI_{LL} and DI_{RR}, are plotted in Fig. 22. For the LHS end-of-span damage indicator, DI_{LL}, it can be seen that the minimum damage level detectable is at least $\delta = 0.08$; and the RHS end-of-span damage indicator, DI_{RR}, again shows reduced damage sensitivity, with the minimum level of damage likely to be detected being $\delta = 0.14$.

6.3. Summary

For convenience, the results of all the sampling methods presented in this section, as well as the no sampling case, are presented in Table 2. These results, which have been ordered in decreasing average annual sample size, N_{year}, firstly, show that the larger sample sizes obtained using peak traffic hours only, offer improved damage detection capability relative to the other sampling methods that do not attempt to maximise traffic volume. Furthermore, these results indicate that the relationship between sample size and damage detection capability is better than reciprocal, i.e. when using an eighth of the number of vehicle crossings, the minimum damage detectable is not eight times worse, it appears to be more like 1.5–2 times worse. Finally, we have given a short summary of the advantages and disadvantages of each sampling method in Table 3.

Table 3
Summary of the advantages and disadvantages of the three sampling methods tested.

Sampling method	Advantages	Disadvantages
Random hourly	• Straightforward to implement as it does not require prior knowledge about expected traffic volumes. • Provides an unbiased sample of the bridge's behaviour.	• Inefficient as might be awake during periods with very little traffic.
Peak traffic hours	• Likely capture the maximum number of vehicle crossings for the same 'on' time. • System 'on' periods are consistent so makes power budget easier to design for.	• Needs accurate traffic data. If the expected traffic data goes out of date, or traffic patterns change, then this method may not be as effective. • Will miss rare or unexpected events that might occur during off-peak hours.
Traffic-volume	• Intended to balance the desire to capture as many vehicle crossings as possible while also capturing these at varying times of the day.	• Needs accurate traffic data. If the expected traffic data goes out of date, or traffic patterns change, then this method may not be as effective.

7. Discussion

The results with no sampling applied (Section 6.1) showed that damage detection was possible down to $\delta = 0.04$ for the LHS end-of-span rotation data (due its closer proximity to the damage at third-span), and $\delta = 0.08$ for the RHS end-of-span.

This demonstrates the effectiveness of our EMD-based damage detection approach, as these levels of detectable damage are lower than those reported for most other rotation-based methods (summarised in Table 1) despite the higher level of confounding effects considered in this study. To improve the robustness of our findings, the numerical simulations used in this study accounted for confounding effects using the following models: (a) seasonal and diurnal bridge stiffness changes using our temperature-capable FE model, (b) a stochastic vehicle arrival model for free-flow traffic with random axle weights and spacings taken from a WIM dataset, and (c) a feature error model was employed to allow for the presence of residual noise and dynamics due to imperfect filtering or inaccuracies in the feature extraction stages.

When sampling was applied in Section 6.2, as expected, the damage detection capability for all three sampling methods was reduced with the minimum detectable damage level increasing. Specifically, the system 'on' time was restricted (12.5 % 'on' time) to model the effect of a power budget constraint, where the three sampling methods were applied to overcome this resource-constraint. Of the three methods tested, the peak traffic hours only sampling method, which captured larger sample sizes, appears to be less penalised being able to detect damages down to $\delta = 0.06$ compared to both the traffic volume probability proportional and naive random hourly sampling methods, which only detected damages down to $\delta = 0.08$. However, it should be noted that even with the penalty associated with an 8x reduction in system 'on' time, these levels of damage are still comparable to those detected by other rotation-based BSHM studies (Table 1).

These initial findings suggest that for a given power budget, sampling strategies that maximise the number of measured vehicle events offer lesser reductions in damage detection performance. For the moment, this has only been shown using long-term numerical simulations for one bridge. Based on engineering judgement, it would seem plausible that employing these methods on other bridges would achieve similar results. However, further work, both numerical simulations and experimental is needed to validate this.

In reality, fully validating this approach would involve field experiments and a situation whereby known damage could be introduced into the bridge during the experiment. Unfortunately, this is not logistically feasible. However, in future work, we hope to do the initial step of this validation to establish that the healthy rotation distributions obtained from long-term (i.e. multi-year) field measurements are in line with the distributions generated via numerical simulations.

Validation of these findings via numerical simulation should involve repeating the methods over a wider variety of scenarios to better characterise the uncertainty in minimum detectable damage levels. Furthermore, future simulation work should consider more fine-grained models, for example, by incorporating a more complex vehicle arrival model that can recreate unique events or outliers, such as heavy traffic during roadworks.

Another possible avenue for future study could be to investigate better means of choosing the baseline from which to compute the EMD. For example, during the initial period of operation more data could be collected to form a 'healthy' reference set. Then, subsequent years could be monitored at a reduced sampling level which helps address the challenge of power sources/batteries degrading over time, as it may be possible to find a more optimal baseline, e.g. from the intersection of the current and reference sets' temperature distributions.

Overall, the numerical simulation results presented in this work demonstrate that knowledge of expected traffic volumes can be beneficial when implementing sampling strategies for BSHM systems, as sampling methods aimed at capturing more vehicle crossings showed better damage detection capability for the same resource usage.

8. Conclusions

This study demonstrated how knowledge of expected traffic volumes could be used to create more efficient sampling methods for long-term rotation-based bridge SHM by capturing more vehicle crossings for the same resource usage, where the system's 'on' time was restricted to simulate a limited energy budget. This paper also introduced an empirically tuned, temperature-capable bridge

finite-element model for long-term simulations, incorporating a stochastic vehicle arrival model and a feature error model to allow for the presence of any residual noise/dynamics due to imperfect filtering or inaccuracies in the feature extraction stages. This allowed us to simulate 60 years worth of bridge rotation monitoring data with varying damage severities to evaluate the impact of environmental and operational variations on our proposed expected traffic volume based sampling methods.

Our EMD-based damage detection approach using maximum end-of-span rotation amplitudes was evaluated using 60 year's worth of bridge rotation data simulated by these models. These results showed a clear detection of damages above $\delta = 0.04$ from the healthy condition using a 95 % PI, which despite the greater degree of confounding effects, is at the lower end of the state of the art in this area (Table 1).

Subsequently, three sampling methods were presented based on: (1) random hourly sampling, (2) peak traffic hours sampling, and (3) expected traffic volume probability proportional sampling. Each method was applied to this simulated long-term bridge data and the performance of our EMD based damage detection method was assessed using the disjoint PI approach. Our findings revealed that whilst employing sampling reduces the sensitivity of damage detection, strategies focusing on capturing the maximum number of vehicle crossings, specifically during peak traffic hours, may yield better results within the same resource constraints. This offers a valuable insight into methods for optimising long-term monitoring strategies for BSHM systems, particularly in resource-constrained settings.

Declaration of competing interest

The authors declare that they have no known competing financial interests or personal relationships that could have appeared to influence the work reported in this paper.

Data availability

Data will be made available on request.

Acknowledgements

The authors gratefully acknowledge the support of the UK Engineering and Physical Sciences Research Council (EPSRC), United Kingdom through the ROSEHIPS project (Grant EP/W005816/1) and a Ph.D. studentship (Grant EP/N509541/1). We are also grateful for use of the computing resources from the Northern Ireland High Performance Computing (NI-HPC) service funded by EPSRC, United Kingdom (Grant EP/T022175). Finally, we would like to thank and acknowledge the Northern Ireland Department for Infrastructure, and in particular Daniel Healy, for their support in arranging the field work.

References

[1] British Standards Institute, UK National Annex for Eurocode – Basis of structural design, 2004.
[2] Highways Agency, Design manual for roads and bridges, volume 3 highway structures: Inspection and maintenance, 2017.
[3] G. Anastasi, M. Conti, M. Di Francesco, A. Passarella, Energy conservation in wireless sensor networks: A survey, Ad Hoc Netw. 7 (3) (2009) 537–568, http://dx.doi.org/10.1016/j.adhoc.2008.06.003.
[4] J. Silva, P. Carvalho, K. Bispo, S. Rito Lima, E-LiteSense: Self-adaptive energy-aware data sensing in WSN environments, Int. J. Commun. Syst. 33 (10) (2020) e4153, http://dx.doi.org/10.1002/dac.4153.
[5] E. OBrien, M. Quilligan, R. Karoumi, Calculating an influence line from direct measurements, Proc. Inst. Civ. Eng. Bridge Eng. 159 (1) (2006) 31–34, http://dx.doi.org/10.1680/bren.2006.159.1.31.
[6] Y. Zeinali, B. Story, Framework for flexural rigidity estimation in Euler–Bernoulli beams using deformation influence lines, Infrastructures 2 (4) (2017) 23, http://dx.doi.org/10.3390/infrastructures2040023.
[7] Y. Zeinali, B. Story, Impairment localization and quantification using noisy static deformation influence lines and Iterative Multi-parameter Tikhonov Regularization, Mech. Syst. Signal Process. 109 (2018) 399–419, http://dx.doi.org/10.1016/j.ymssp.2018.02.036.
[8] D. Hester, J. Brownjohn, F. Huseynov, E. Obrien, A. Gonzalez, M. Casero, Identifying damage in a bridge by analysing rotation response to a moving load, Struct. Infrastruct. Eng. 16 (7) (2020) 1050–1065, http://dx.doi.org/10.1080/15732479.2019.1680710.
[9] F. Huseynov, C. Kim, E. OBrien, J. Brownjohn, D. Hester, K. Chang, Bridge damage detection using rotation measurements – Experimental validation, Mech. Syst. Signal Process. 135 (2020) 106380, http://dx.doi.org/10.1016/j.ymssp.2019.106380.
[10] M. Alamdari, K. Kildashti, B. Samali, H. Goudarzi, Damage diagnosis in bridge structures using rotation influence line: Validation on a cable-stayed bridge, Eng. Struct. 185 (2019) 1–14, http://dx.doi.org/10.1016/j.engstruct.2019.01.124.
[11] E. Oskoui, T. Taylor, F. Ansari, Method and sensor for monitoring weight of trucks in motion based on bridge girder end rotations, Struct. Infrastruct. Eng. 16 (3) (2020) 481–494, http://dx.doi.org/10.1080/15732479.2019.1668436.
[12] E. OBrien, J. Brownjohn, D. Hester, F. Huseynov, M. Casero, Identifying damage on a bridge using rotation-based Bridge Weigh-In-Motion, J. Civ. Struct. Health Monit. (2020) http://dx.doi.org/10.1007/s13349-020-00445-w.
[13] Y.-T. Wei, T.-H. Yi, D.-H. Yang, H.-N. Li, Bridge Damage Localization Using Axle Weight Time History Data Obtained through a bridge weigh-in-motion system, J. Perform. Constr. Facil. 35 (5) (2021) 04021065, http://dx.doi.org/10.1061/(asce)cf.1943-5509.0001642.
[14] J. Sinha, M. Friswell, S. Edwards, Simplified models for the location of cracks in beam structures using measured vibration data, J. Sound Vib. 251 (1) (2002) 13–38, http://dx.doi.org/10.1006/jsvi.2001.3978.
[15] A. Ferguson, D. Hester, R. Woods, A direct method to detect and localise damage using longitudinal data of ends-of-span rotations under live traffic loading, J. Civ. Struct. Health Monit. (2021) http://dx.doi.org/10.1007/s13349-021-00533-5.
[16] A. Ramdas, N. Garcia, M. Cuturi, On wasserstein two sample testing and related families of nonparametric tests, 2015, arXiv:1509.02237 [math, stat].
[17] E. Levina, P. Bickel, The Earth Mover's distance is the Mallows distance: Some insights from statistics, in: Proceedings of the IEEE International Conference on Computer Vision, Vol. 2, 2001, pp. 251–256, http://dx.doi.org/10.1109/iccv.2001.937632.

[18] A. González, D. Hester, An investigation into the acceleration response of a damaged beam-type structure to a moving force, J. Sound Vib. 332 (13) (2013) 3201–3217, http://dx.doi.org/10.1016/j.jsv.2013.01.024.
[19] D. Hester, A. González, A wavelet-based damage detection algorithm based on bridge acceleration response to a vehicle, Mech. Syst. Signal Process. 28 (2012) 145–166, http://dx.doi.org/10.1016/j.ymssp.2011.06.007.
[20] W. Zhang, H. Ma, J. Zeng, S. Wu, B. Wen, Vibration responses analysis of an elastic-support cantilever beam with crack and offset boundary, Mech. Syst. Signal Process. 95 (2017) 205–218, http://dx.doi.org/10.1016/j.ymssp.2017.03.032.
[21] B. Peeters, G. De Roeck, One-year monitoring of the Z24-bridge: Environmental effects versus damage events, Earthq. Eng. Struct. Dyn. 30 (2) (2001) 149–171, http://dx.doi.org/10.1002/1096-9845(200102)30:2<149::aid-eqe1>3.0.co;2-z.
[22] British Standards Institution, Eurocode 1: Actions on structures. Part 2 Part 2, 2010.
[23] C. O'Higgins, D. Hester, W. Ao, P. McGetrick, D. Robinson, Inherent uncertainty in the extraction of frequencies from time domain signals, Infrastruct. Asset Manag. (2019) 1–10, http://dx.doi.org/10.1680/jinam.19.00058.
[24] B. Peeters, System Identification and Damage Detection in Civil Engineering (Ph.D. thesis), Katholieke Universiteit Leuven, Leuven, Belgium, 2000.
[25] Met Office, Met office MIDAS open: UK land surface stations data (1853-current), 2019.
[26] Y. Ni, H. Zhou, J. Ko, Generalization capability of neural network models for temperature-frequency correlation using monitoring data, J. Struct. Eng. 135 (10) (2009) 1290–1300, http://dx.doi.org/10.1061/(ASCE)ST.1943-541X.0000050.
[27] A. Banerjee, J. Dolado, J. Galbraith, D. Hendry, A. Banerjee, J. Dolado, J. Galbraith, D. Hendry, Co-Integration, Error Correction, and the Econometric Analysis of Non-Stationary Data, in: Advanced Texts in Econometrics, Oxford University Press, Oxford, New York, 1993.
[28] M. Hatanaka, M. Hatanaka, Time-Series-Based Econometrics: Unit Roots and Co-Integrations, in: Advanced Texts in Econometrics, Oxford University Press, Oxford, New York, 1996.
[29] F. Hampel, A general qualitative definition of robustness, The annals of mathematical statistics 42 (6) (1971) 1887–1896, http://dx.doi.org/10.1214/aoms/1177693054.
[30] B. Iglewicz, D. Hoaglin, How to Detect and Handle Outliers, in: ASQC Basic References in Quality Control, no. v. 16, ASQC Quality Press, Milwaukee, Wis, 1993.
[31] W. Adams, Road traffic considered as a random series. (Includes plates), J. Inst. Civ. Eng. 4 (1) (1936) 121–130, http://dx.doi.org/10.1680/ijoti.1936.14802.
[32] D. Gerlough, A. Schuhl, Use of Poisson Distribution in Highway Traffic, Eno Foundation for Highway Traffic Control Saugatuck, CT, 1955.
[33] L. Breiman, The Poisson tendency in traffic distribution, Ann. Math. Stat. 34 (1) (1963) 308–311, http://dx.doi.org/10.1214/aoms/1177704267.
[34] Transport Infrastructure Ireland, WIM Data 2014 - data.gov.ie, https://data.gov.ie/dataset/wim-data-2014.